1360

FEARS STRUCTURAL ENGINEERING LABORATORY

School of Civil Engineering and Environmental Science
University of Oklahoma
Norman, Oklahoma 73019

00630

SPLICE RESEARCH
Progress Report
ANALYTICAL AND EXPERIMENTAL
INVESTIGATION OF THE EXTENDED
STIFFENED MOMENT END-PLATE CONNECTION
WITH FOUR BOLTS AT THE
BEAM TENSION FLANGE

by
Scott J. Morrison
and
Abolhassan Astaneh-Asl
Thomas M. Murray
Co-Principal Investigators

Sponsored by
Metal Building Manufacturers Association
and
American Institute of Steel Construction

Report No. FSEL/MBMA 85-05

December 1985

FEARS STRUCTURAL ENGINEERING LABORATORY
School of Civil Engineering and Environmental Science
University of Oklahoma
Norman, Oklahoma 73019

TABLE OF CONTENTS

00632

LIST OF FIGURES

LIST OF TABLES

ANALYTICAL AND EXPERIMENTAL INVESTIGATION OF THE EXTENDED STIFFENED MOMENT END-PLATE CONNECTION WITH FOUR BOLTS AT THE BEAM TENSION FLANGE

CHAPTER I

INTRODUCTION

1.1 Background

Moment end-plate connections are commonly used in steel portal frame construction as bolted moment-resistant connections. The moment end-plate is typically used to connect a beam to a beam, often referred to as a "splice-plate connection", Figure 1.1(a), or to connect a beam to a column, Figure 1.1(b).

Several design procedures for various moment end-plate configurations have been suggested to determine end-plate thickness and bolt diameter based on results from finite-element method, yield-line theory, or experimental test data. Unfortunately, these procedures produce a variety of values for end-plate thickness and bolt diameter for the same design example. For one particular configuration and loading, the variance of design end-plate thickness exceeded 100% [1]. An even greater variation was found for bolt force prediction, as some methods assume prying action is negligible, whereas other methods assume prying action is significant and contributes substantially to bolt force.

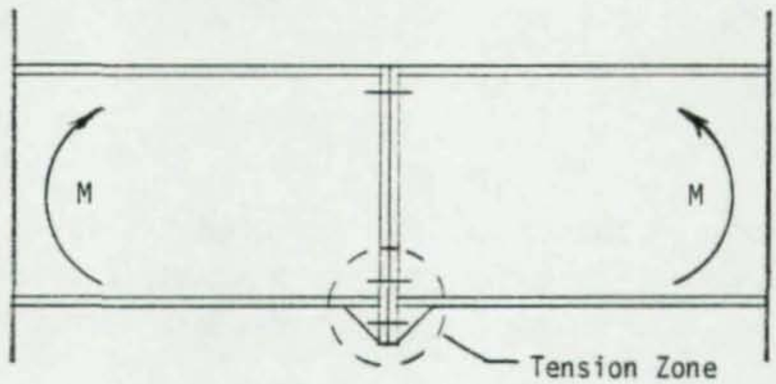

(a) Beam-to-Beam Connection

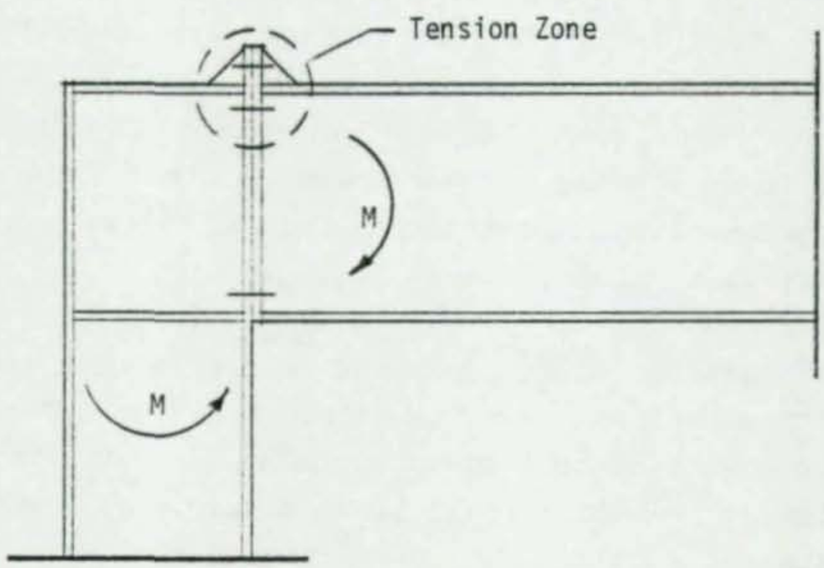

(b) Beam-to-Column Connection

Figure 1.1 Typical Uses of Moment End-Plate Connections

Hendrick et al [2] has finalized a unification of design procedures for four configurations of the flush type moment end-plate connection. Two of these flush type connections are unstiffened: the two-bolt unstiffened, Figure 1.2(a), and the four-bolt unstiffened, Figure 1.2(b). The other two flush type connections are stiffened: the four-bolt stiffened with web gusset plate between the two tension bolt rows, Figure 1.2(c), and the four-bolt stiffened with web gusset plate outside the two tension bolt rows, Figure 1.2(d). The gusset plates for each of the flush stiffened connections are symmetrical about the beam web and are welded to the end-plate and the beam web.

This report continues the unification of design procedures for moment end-plate connections established by Hendrick et al [2] for another configuration of moment end-plate. This fifth configuration is the four-bolt extended stiffened form shown in Figure 1.3. In this connection, the four bolts in the tension region are placed one row of two bolts on each side of the beam tension flange. A triangular stiffener is located on the end-plate extension outside of the beam depth on the beam web centerline. The stiffener is welded to both the end-plate and the outside of the beam flange. The unified design procedures include determination of end-plate thickness and prediction of bolt forces.

1.2 Literature Review

An extensive review of end-plate connection literature was reported by Srouji et al [1]. They presented the design procedures of various authors and made comparisons of end-plate design thickness based on those authors' recommendations. Based on the review, they selected the yield-line method for end-plate analysis and the Kennedy et al method [3] for bolt force prediction. These approaches

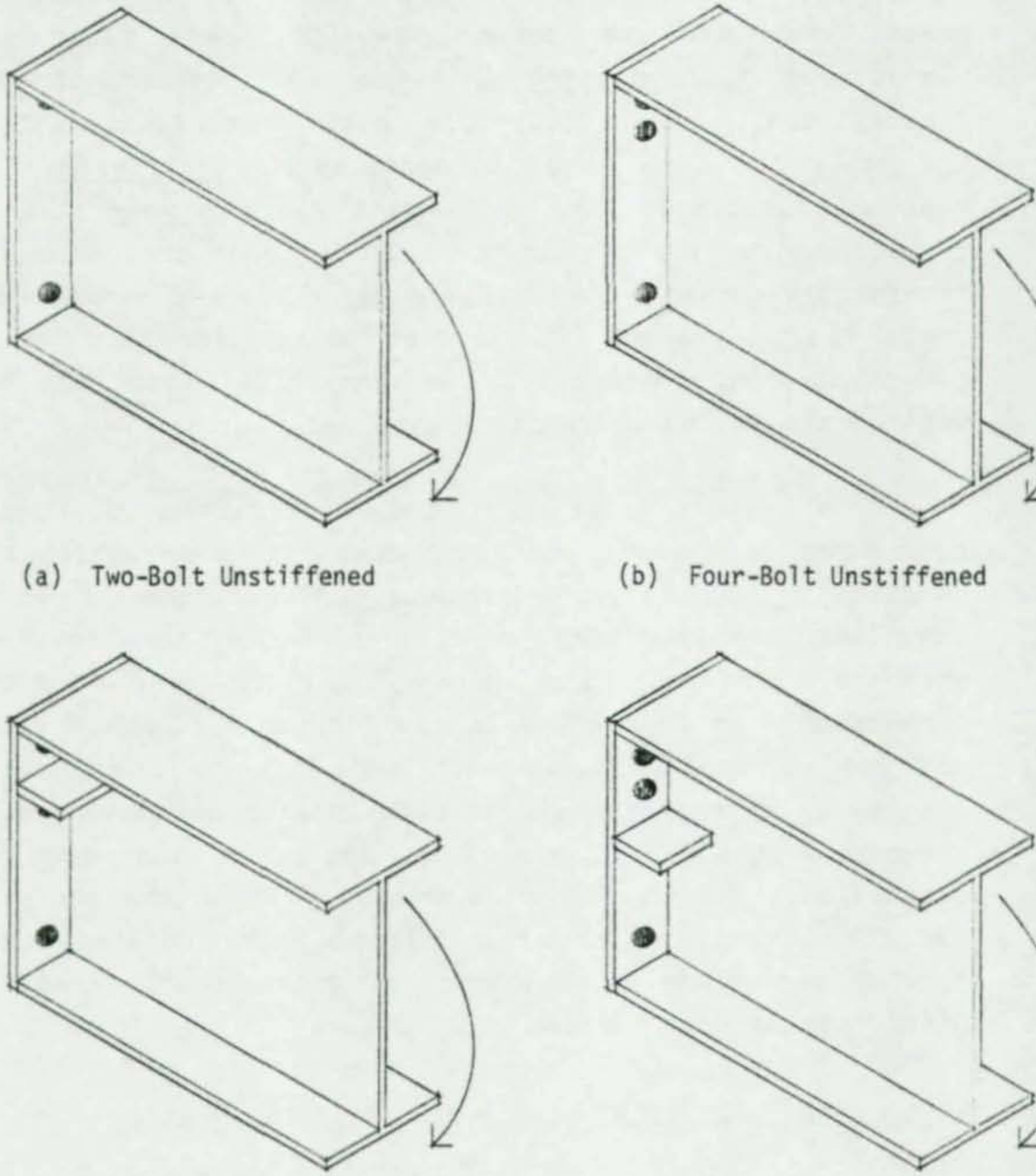

(a) Two-Bolt Unstiffened

(b) Four-Bolt Unstiffened

(c) Four-Bolt Stiffened with Web Gusset Plate <u>Between</u> the Tension Bolt <u>Rows</u>

(d) Four-Bolt Stiffened with Web Gusset Plate <u>Outside</u> the Tension Bolt <u>Rows</u>

Figure 1.2 Four Flush Type Configurations of Moment End-Plate Connections (Unification Finalized by Hendrick _et al_ (2))

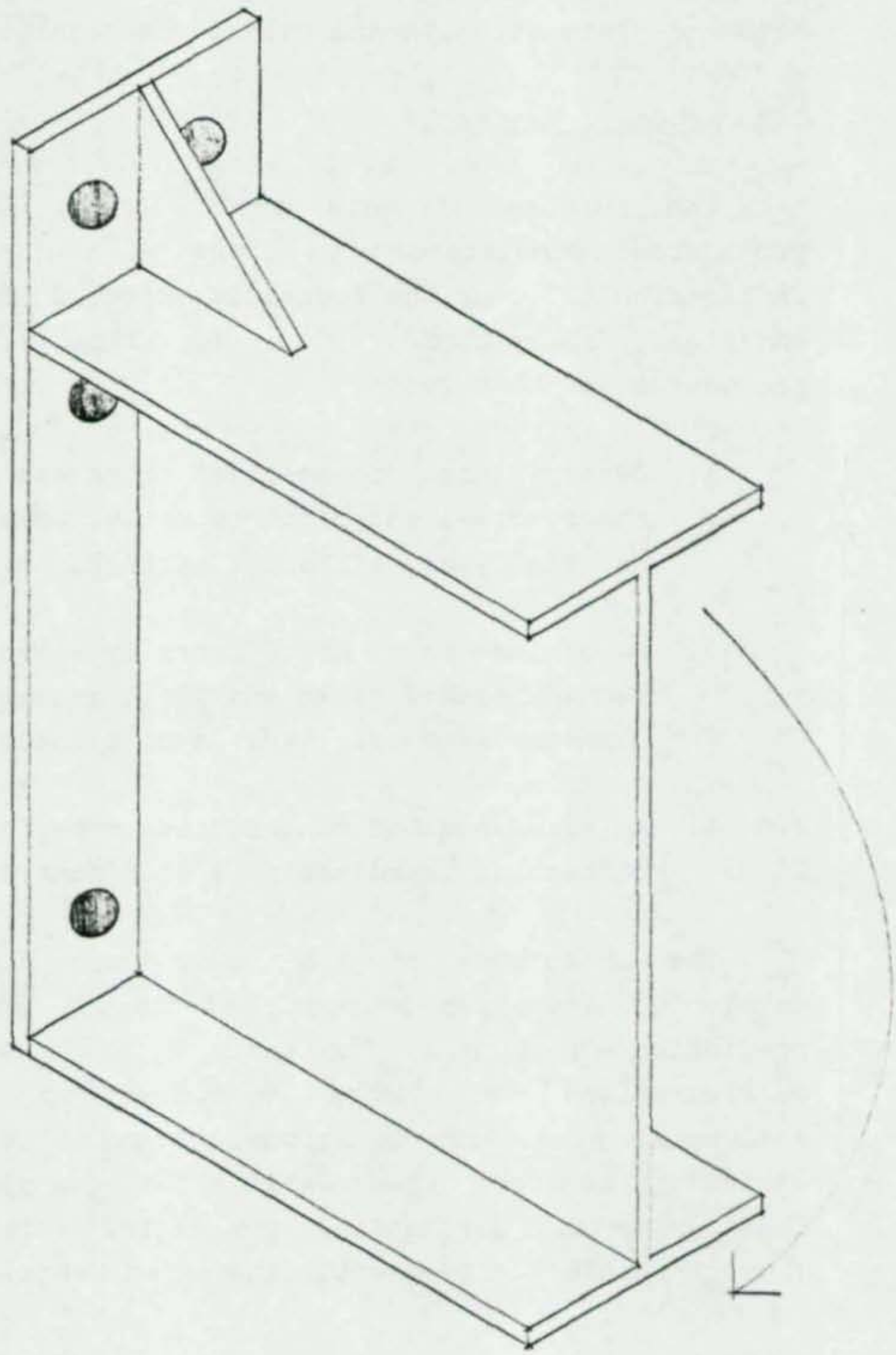

Figure 1.3 Four-Bolt Extended Stiffened Moment End-Plate Connection

were adopted for the present study because of the successful correlation of prediction and experimental test results for both end-plate strength and bolt force magnitude.

1.3 Scope of Research

The purpose of this study is to develop design procedures, consistent with those of the Hendrick et al unification [2], for the four-bolt extended stiffened moment end-plate connection. More specifically, the design procedures are to provide:

1. Determination of end-plate thickness by yield-line theory given end-plate geometry, beam geometry, and material yield stress; a strength criterion.

2. Determination of bolt forces by a modified Kennedy method given end-plate geometry, bolt diameter, and bolt type; a bolt force criterion.

3. An assessment of construction type for which the connection is suitable; a stiffness criterion.

The objectives of the study were accomplished by developing end-plate strength prediction and bolt force prediction equations. Six tests of full size end-plate configurations were then conducted to verify these analytical prediction equations. Figure 1.4 presents the various parameters that define the end-plate geometry. These geometric parameters were varied within the limits shown in Table 1.1 to develop the experimental test matrix.

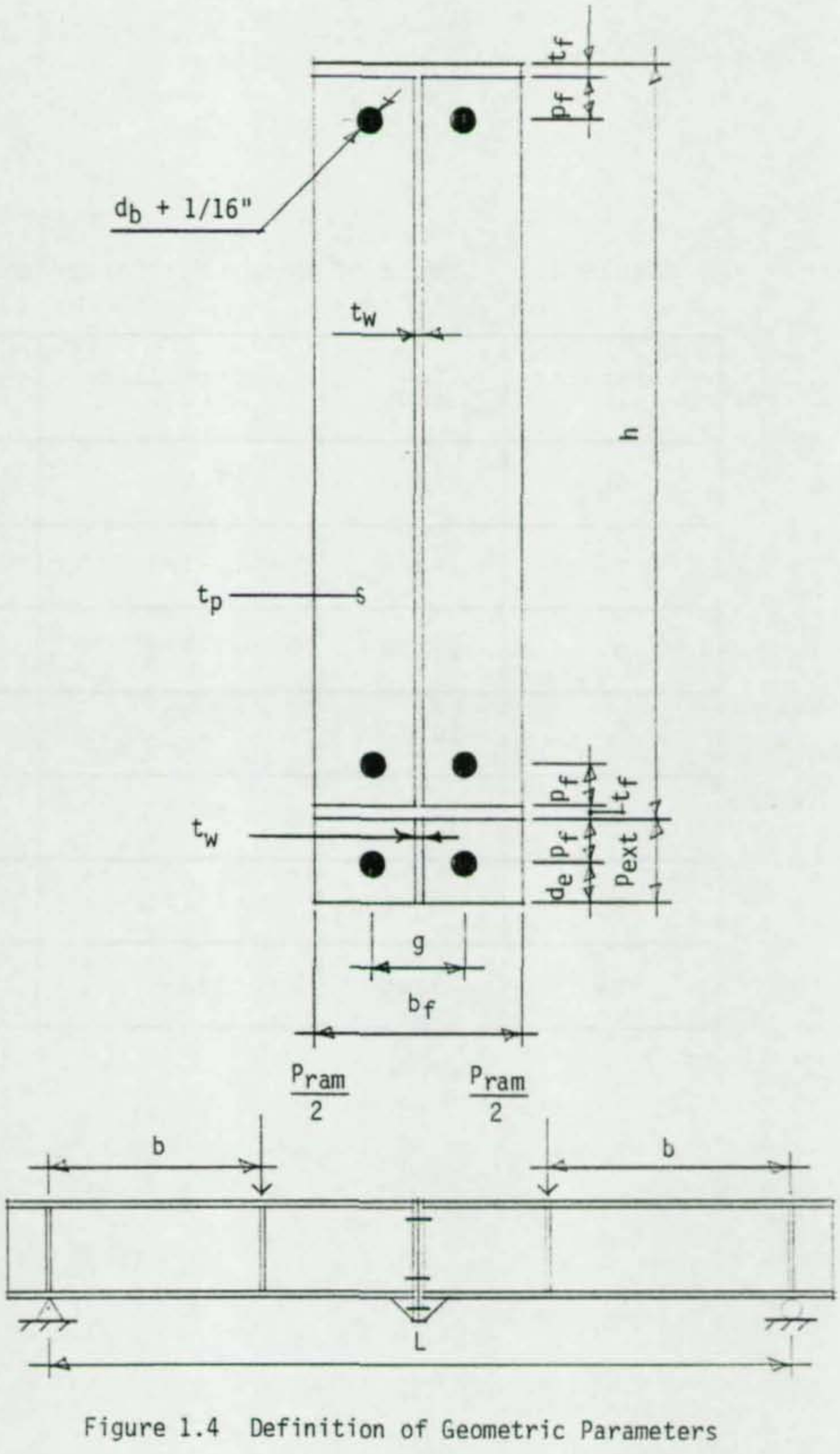

Figure 1.4 Definition of Geometric Parameters

Table 1.1 Limits of Geometric Parameters

Parameter	Low (in)	Intermediate (in)	High (in)
d_b	5/8	7/8	1-1/4
p_f	1-1/8	1-3/4	2-1/2
g	2-1/4	3-7/8	5-1/2
h	10	20	30
b_f	5	7	10
t_w	12 gage	3/16	3/8
t_f	7 gage	3/8	1/2

CHAPTER II
ANALYTICAL STUDY

2.1 Yield-Line Theory

Yield-lines are the continuous formation of plastic hinges along a straight or curved line. It is assumed that yield-lines divide a plate into rigid plane regions since elastic deformations are negligible when compared with plastic deformations. The failure mechanism of the plate exists when yield-lines form a kinematically valid collapse mechanism. Most of the yield-line theory development is related to reinforced concrete; nonetheless, the principles and findings are also applicable to steel plates.

The analysis of a yield-line mechanism can be performed by two different methods, the equilibrium method and the virtual work or energy method. The latter method is more suitable for the end-plate application and is used herein. In this method, the external work done by the applied load, in moving through a small arbitrary virtual deflection field, is equated to the internal work done as the plate rotates at the yield lines to facilitate this virtual deflection field. For a selected yield-line pattern and loading, a specific plastic moment is required along these hinge lines. For the same loading, other patterns may result in a larger required plastic moment capacity. Hence, the appropriate pattern is that which requires the largest required plastic moment. Conversely, for a given plastic moment capacity, the appropriate mechanism is that which produces the smallest failure load. This implies that the yield-line theory is an upper bound procedure; therefore, one must find the least upper bound.

The procedure to determine an end-plate plastic moment capacity, or failure load, is to first arbitrarily select possible yield-line mechanisms. Next, equate the external and internal work, thereby establishing the relationship between the applied load and the ultimate resisting moment. This equation is then solved for either the unknown load or the unknown resisting moment. By comparing the values obtained from the arbitrarily selected mechanisms, the appropriate yield-line mechanism is that with the largest required plastic moment capacity or the smallest failure load. A more detailed description is presented by Hendrick et al [2].

Two yield-line mechanisms, shown in Figure 2.1, are appropriate for the four-bolt extended stiffened moment end-plate. These mechanisms, or patterns, depend on the length of the end-plate extension outside of the beam depth. The particular length of the end-plate extension determines whether or not a hinge line forms at the extreme edge of the end-plate. The first case, in which a hinge line does form near the outside edge of the end-plate, is denoted as Case 1, Figure 2.1(a), and the second case in which no hinge line forms above the outside bolt line is denoted as Case 2, Figure 2.1(b). To determine which pattern controls, the unknown dimension s must be determined. The s dimension is found by differentiating the internal work expression with respect to s and equating to zero. The resulting expression for s is:

$$s = (1/2)\sqrt{b_f g} \tag{2.1}$$

The equations for the Case 1 and Case 2 mechanisms can be written for the ultimate moment capacity of the

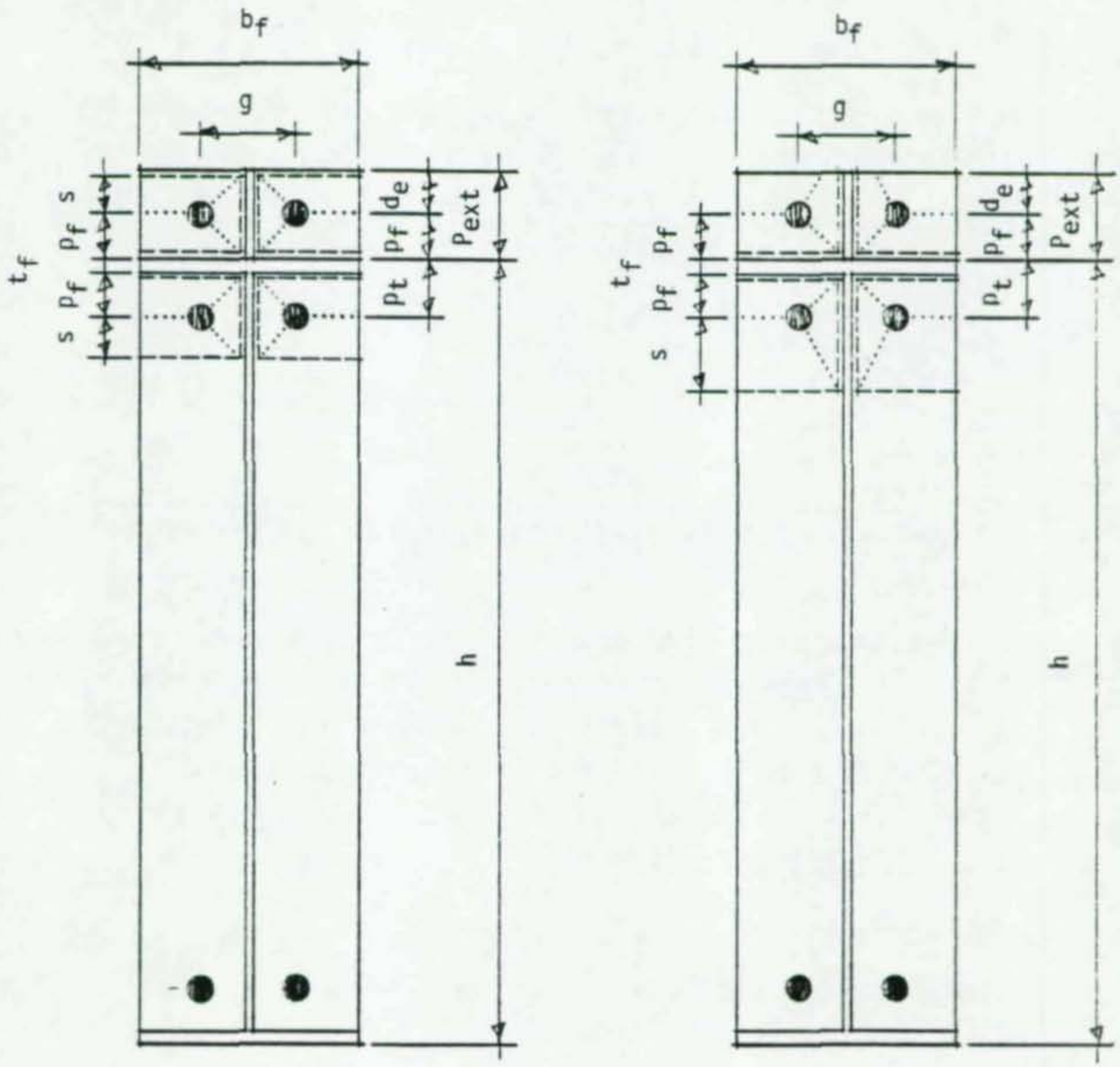

(a) Case 1 when $s<d_e$

(b) Case 2 when $s>d_e$

Figure 2.1 Yield-Line Mechanisms for the Four-Bolt Extended Stiffened Moment End-Plate Connection end-plate, M_u, or when rearranged, for the required end-plate thickness, t_p.

For Case 1 when $s < d_e$:

$$M_u = 4m_p\{[(b_f/2)(1/p_f+1/s)+(p_f+s)(2/g)][(h-p_t)+(h+p_f)]\} \quad (2.2)$$

$$t_p = \left\{\frac{M_u/F_{py}}{[(b_f/2)(1/p_f+1/s)+(p_f+s)(2/g)][(h-p_t)+(h+p_f)]}\right\}^{\frac{1}{2}} \quad (2.3)$$

For Case 2 when $s > d_e$:

$$M_u = 4m_p\{[(b_f/2)(1/p_f+1/2s)+(p_f+d_e)(2/g)][(h-p_t)+(h+p_f)]\} \quad (2.4)$$

$$t_p = \left\{\frac{M_u/F_{py}}{[(b_f/2)(1/p_f+1/2s)+(p_f+d_e)(2/g)][(h-p_t)+(h+p_f)]}\right\}^{\frac{1}{2}} \quad (2.5)$$

A photo of an observed yield-line pattern for the four-bolt extended stiffened moment end-plate is shown in Figure 2.2. The yield-line pattern is indicated by the flaking of "white wash" from the test specimen.

2.2 Bolt Force Predictions

Yield-line theory does not produce bolt force predictions including prying action forces. Since experimental results indicate that prying action behavior is present in end-plate connections, a method suggested by Kennedy et al [3] was adopted to predict bolt forces as a function of applied flange force.

The Kennedy method is based on the split-tee analogy and three stages of plate behavior. Consider a split-tee model, Figure 2.3, consisting of a flange bolted to a rigid support and attached to a web through which a tension load is applied. At the lower levels of applied load, the flange

Figure 2.2 Photo of Test Specimen Yield-Line Pattern

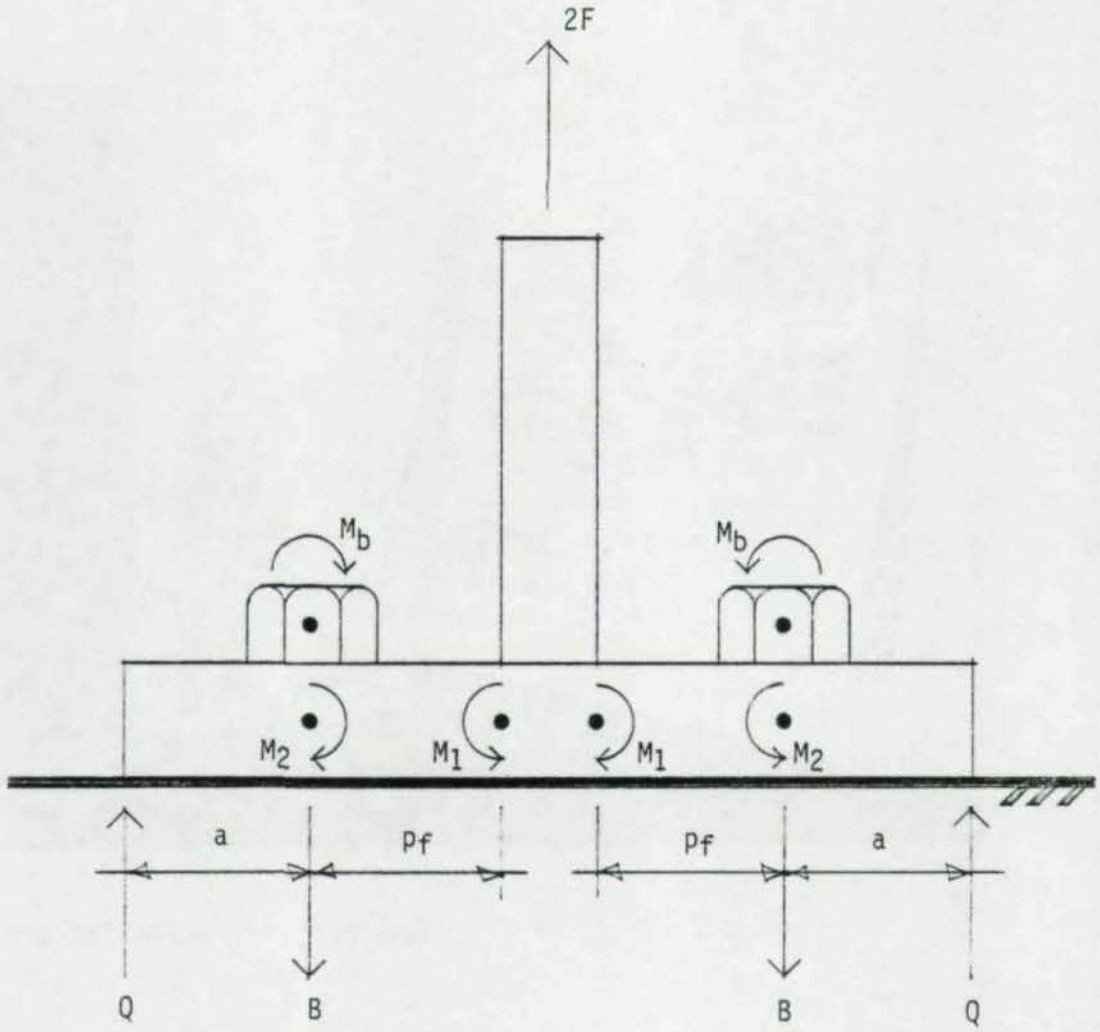

Figure 2.3 Kennedy Method Split-Tee Model

behavior is termed thick plate behavior as plastic hinges have not formed in the split-tee flange, Figure 2.4(a). As the applied load is increased, two plastic hinges form at the centerline of the flange and each web face intersection, Figure 2.4(b). This yielding marks the "thick plate limit" and indicates the second stage of plate behavior termed intermediate plate behavior. At a greater applied load level, two additional plastic hinges form at the centerline of the flange and each bolt, Figure 2.4(c). The formation of this second set of plastic hinges marks the "thin plate limit" and indicates the third stage of plate behavior termed thin plate behavior.

For all stages of plate behavior, the Kennedy method predicts a bolt force as the sum of a portion of the applied force and a prying force. The portion of the applied force depends on the applied load, while the magnitude of the prying force depends on the stage of plate behavior. For the first stage of behavior, or thick plate behavior, the prying force is zero. For the second stage of behavior, or intermediate plate behavior, the prying force increases from zero at the thick plate limit to a maximum at the thin plate limit. For the third stage of behavior, or thin plate behavior, the prying force is maximum and constant. The distance "a" between the point of prying force application and the centerline of bolt has been determined empirically by Hendrick *et al* [2] for the flush end-plate configurations shown in Figure 1.2, as a function of t_p/d_b:

$$a = 3.682\,(t_p/d_b)^3 - 0.085 \qquad (2.6)$$

Modifications of the Kennedy method are necessary for application to the four-bolt extended stiffened moment end-plate connection. First, the connection is idealized in two parts: the outer end-plate and the inner end-plate, Figure 2.5. The outer end-plate consists of the end-plate exten-

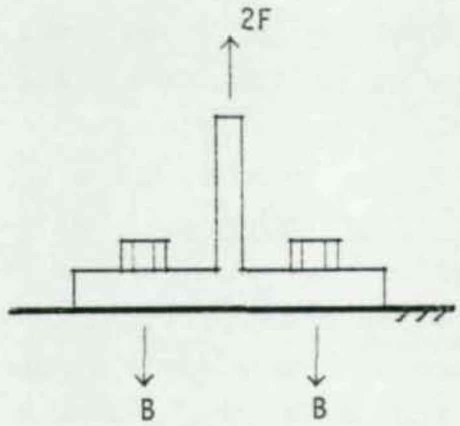

(a) First Stage / Thick Plate Behavior

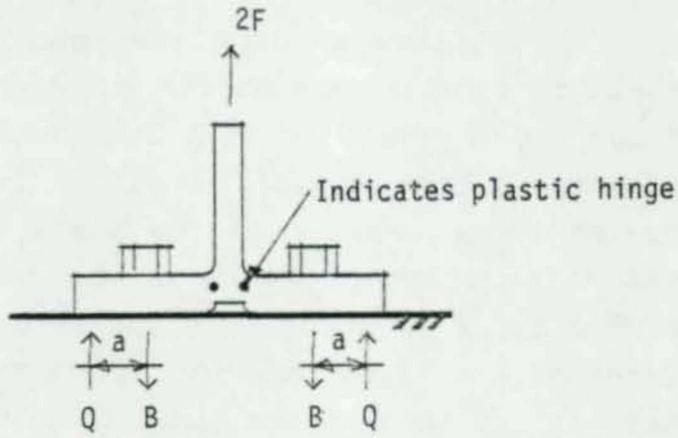

(b) Second Stage / Intermediate Plate Behavior

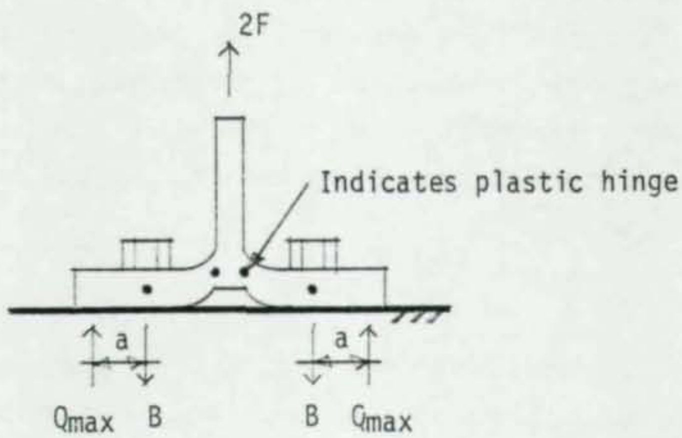

(c) Third Stage / Thin Plate Behavior

Figure 2.4 Kennedy Method Split-Tee Behavior

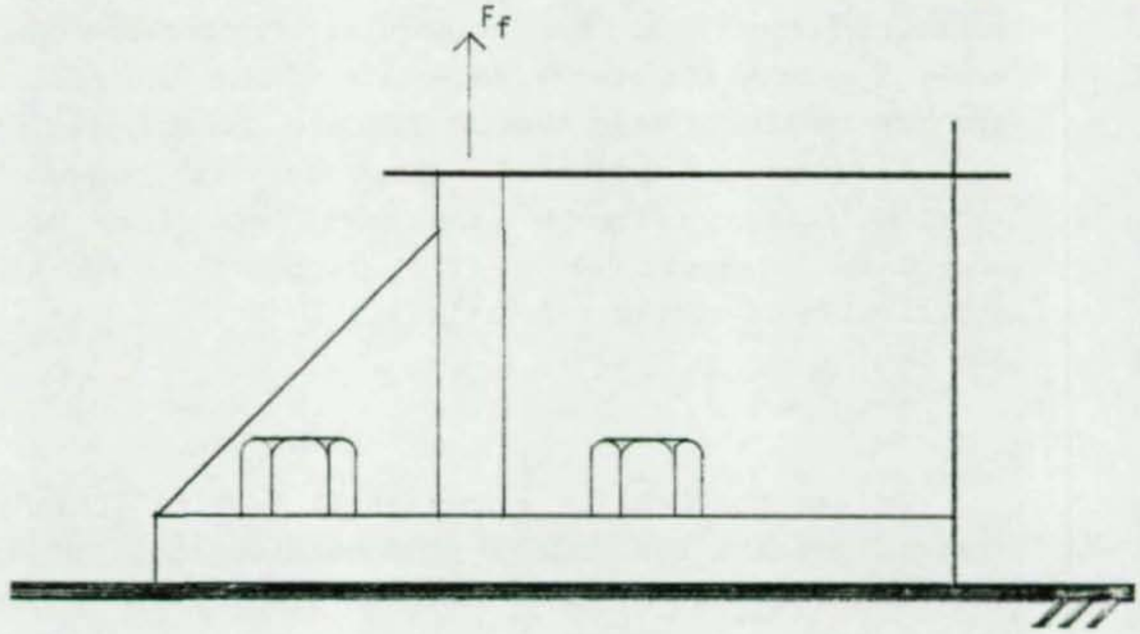

(a) End-Plate at the Beam Tension Flange

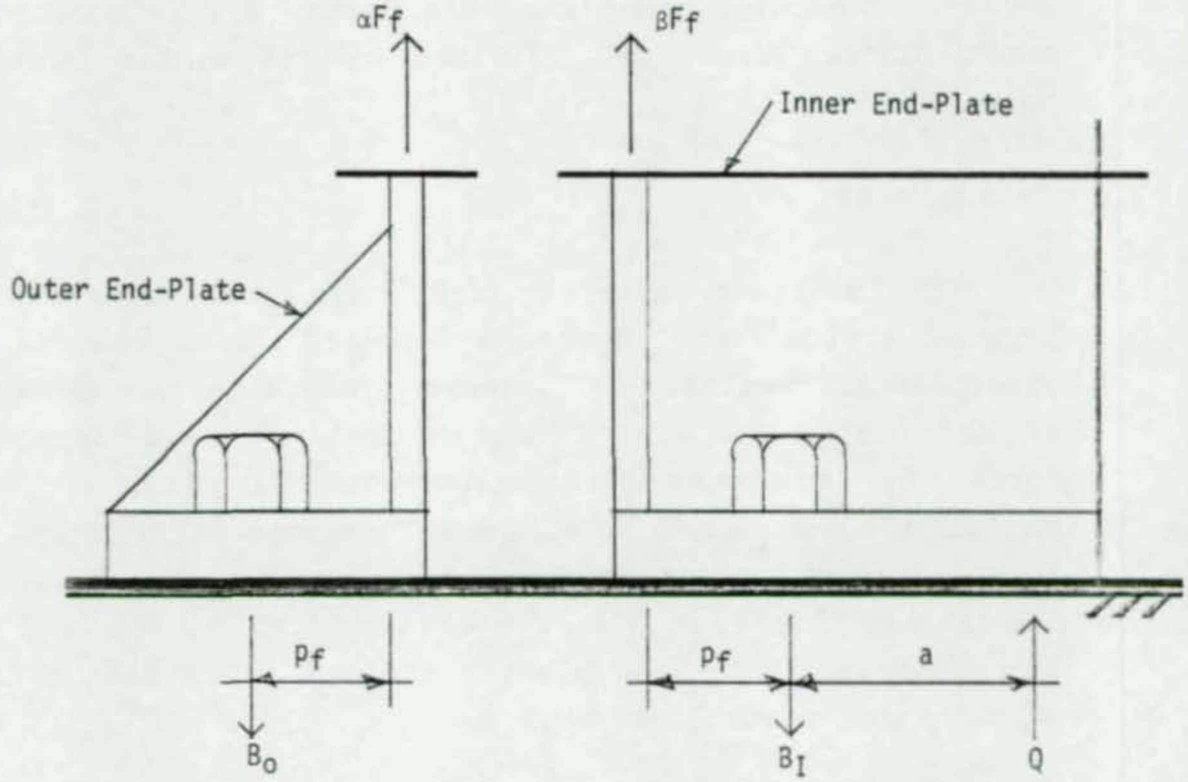

(b) Idealization of the End-Plate at the Beam Tension Flange

Figure 2.5 Modified Kennedy Method Idealization for the Four-Bolt Extended Stiffened Moment End-Plate Connection sion outside the beam tension flange, a portion of the beam tension flange, and the triangular stiffener. The inner end-plate consists of the end-plate within the beam flanges and the remaining beam tension flange. Second, two factors, α and β, are introduced. These factors proportion the tension flange force to the outer end-plate and inner end-plate, respectively. The factors α and β were empirically developed and satisfy:

$$\alpha + \beta = 1.0 \tag{2.7}$$

It was observed in experimental testing (Chapter III) that no contact was made at the outside edges of the two outer end-plates in beam-to-beam connections. Since no contact was made, no prying action is possible. Thus, the outer end-plate behavior is thick at all applied load levels. The outer end-plate bolt force, B_o, is simply the outer flange force, αF_f, divided by the number of outer bolts, 2:

$$B_o = \alpha F_f / 2 \tag{2.8}$$

The inner end-plate, on the other hand, does exhibit prying action at increased applied load levels in experimental testing. In order to determine the magnitude of the prying force, and hence, the inner end-plate bolt force, B_I, one must first ascertain the stage of inner end-plate behavior. The inner end-plate behavior is established by comparing the inner flange force, βF_f, with the flange force at the thick plate limit, F_1, and the flange force at the thin plate limit, F_{11}. The flange force at the thick plate limit, F_1, is:

$$F_1 = \frac{b_f t_p^2 F_{py}}{4p_f \sqrt{1 + (3t_p^2/16p_f^2)}} \tag{2.9}$$

The flange force at the thin plate limit, F_{11}, is:

$$F_{11} = \frac{t_p^2\ F_{py}\ [0.85(b_f/2) + 0.80\ w'] + [(\pi d_b^3 F_{yb})/8]}{2p_f} \quad (2.10)$$

If the inner flange force, βF_f, is less than the flange force at the thick plate limit, F_1, the end-plate behaves as a thick plate and the prying force is zero. Hence, the inner bolt force, B_I, for thick plate behavior is the inner flange force, βF_f, divided by the number of inner bolts, 2:

$$B_I = \beta F_f\ /\ 2 \quad \text{when } \beta F_f < F_1 \quad (2.11)$$

If the inner flange force, βF_f, is greater than or equal to the flange force at the thick plate limit, F_1, and less than or equal to the flange force at the thin plate limit, F_{11}, the end-plate behavior is intermediate and the prying force is between zero and a maximum. The prying force, Q, for this case is:

$$Q = \frac{\beta F_f p_f}{2a} - \frac{\pi d_b^3 F_{yb}}{32a} - \frac{b_f t_p^2}{8a} \sqrt{F_{py}^2 - 3(\beta F_f / b_f t_p)^2} \quad (2.12)$$

Hence, the inner bolt force, B_I, for intermediate end-plate behavior is the inner flange force, βF_f, divided by the number of inner bolts, 2, plus the prying force, Q:

$$B_I = \beta F_f\ /\ 2 + Q \quad \text{when } F_1 \le \beta F_f \le F_{11} \quad (2.13)$$

Finally, if the inner flange force, βF_f, is greater than the flange force at the thin plate limit, F_{11}, the end-plate behavior is thin and the prying force is at a maximum. The prying force, Q_{max}, is:

$$Q_{max} = \frac{w' t_p^2}{4a} \sqrt{F_{py}^2 - 3(F'/w' t_p)^2} \quad (2.14)$$

The F' term in the Q_{max} expression is the lesser of:

$$F_{limit} = F_{11} / 2 \qquad (2.15)$$

or

$$F_{max} = \beta F_f / 2 \qquad (2.16)$$

Hence, the inner bolt force, B_I, for thin end-plate behavior is the inner flange force, βF_f, divided by the number of inner bolts, 2, plus the prying force, Q_{max}:

$$B_I = \beta F_f / 2 + Q_{max} \quad \text{when } \beta F_f > F_{11} \qquad (2.17)$$

The reader is cautioned that the quantities under the radicals in Equations 2.12 and 2.14 can be negative. A negative value for these terms indicates that the end-plate locally yielded in shear before the bolt prying action force could be developed, thus the connection is not adequate for the applied load.

2.3 Moment-Rotation Relationships

Connection stiffness is the rotational resistance of a connection to applied moment. This connection characteristic is often described with a moment versus rotation or M-Φ diagram, Figure 2.6. The slope of the M-Φ curve, typically obtained from experimental test data, is an indication of the rotational stiffness of the connection. The greater the slope of the curve; the greater the stiffness of the connection.

This stiffness is reflected in the three types of construction recognized by the AISC Specification: Type I, Type II, and Type III. Type I Construction, or rigid framing, assumes that the connections have sufficient

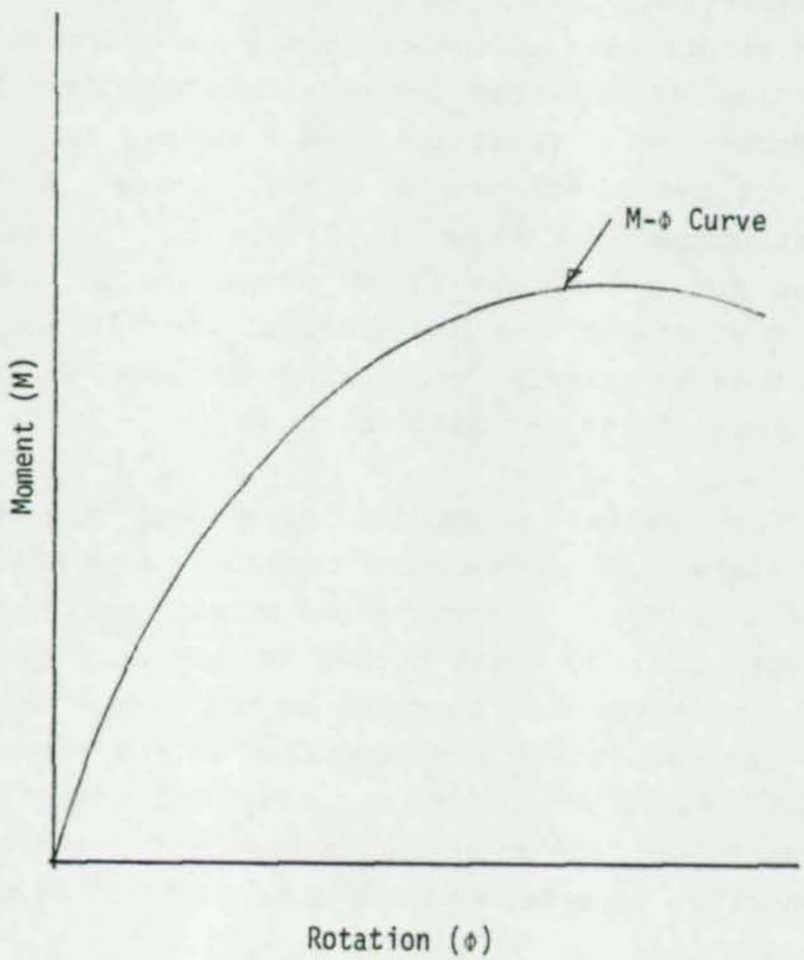

Figure 2.6 Typical M-Φ Diagram

rigidity to fully resist rotation at joints and is unconditionally permitted. Type II Construction, or simple framing, assumes that the connections are free to rotate under gravity load, that beams are connected for shear only, and that connections and connected members have adequate capacity to resist wind moments. Finally, Type III Construction, or semi-rigid framing, assumes that connections have a dependable and known moment capacity as a function of rotation between that of Type I and Type II Construction. Idealized M-Φ curves for three typical connections representing the three AISC types of construction are shown in Figure 2.7. Note that the M-Φ curve for an ideally fixed connection is one which traces the ordinate of the M-Φ diagram, whereas the M-Φ curve for an ideally simple connection is one which traces the abscissa of the M-Φ diagram.

For beams, guidelines have been suggested [6,7] to correlate M-Φ connection behavior and AISC Construction Type. A Type I connection should carry an end moment greater than or equal to 90% of the full fixity end moment and not rotate more than 10% of the simple span rotation. A Type II connection should resist an end moment less than or equal to 20% of the full fixity end moment and rotate at least 80% of the simple span beam end rotation. A Type III connection lies between the limits of the Type I and Type II connections.

The simple span beam end rotation for any loading is given by:

$$\Theta_S = M_F L/2EI \tag{2.18}$$

Then, assuming M_F is the yield moment of the beam, sF_Y, and with $I/s = h/2$:

$$\Theta_S = F_Y L/Eh \tag{2.19}$$

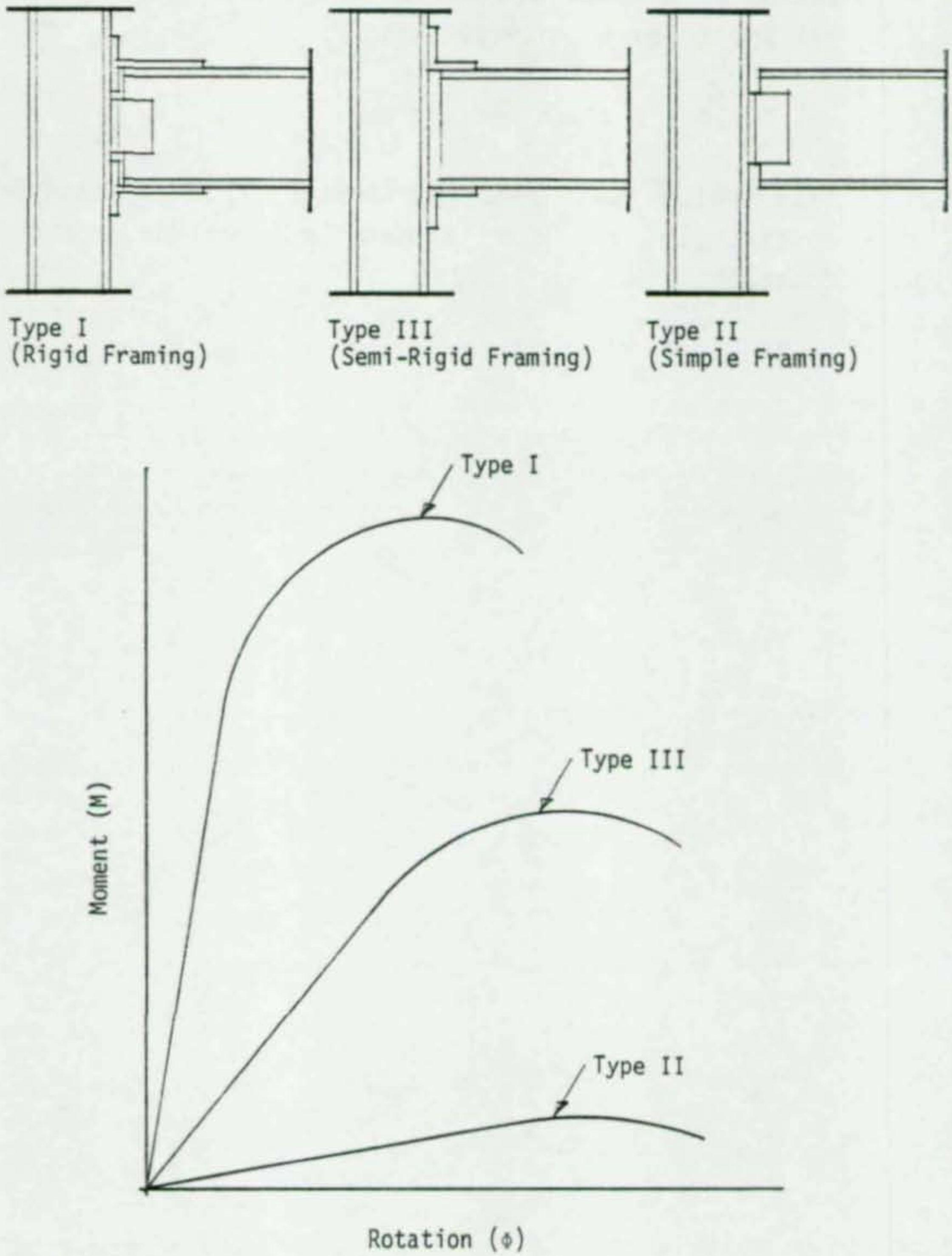

Figure 2.7 Idealized M-Φ Curves for Typical Connections

Taking as a limit L/h equal to 24, and with F_y equal to 50 ksi and E equal to 29,000 ksi:

$$0.1\Theta_s = 0.00414 \text{ radians} \tag{2.20}$$

This value is used in Section 4.3 to determine the suitability of the tested connections for Type I Construction.

CHAPTER III

EXPERIMENTAL INVESTIGATION

3.1 Test Setup and Procedure

A series of six tests were performed to verify the yield-line theory and modified Kennedy method predictions for the four-bolt extended stiffened moment end-plate connection. The test specimens consisted of end-plates welded to two beam sections which were in turn bolted together in the beam-to-beam connection configuration shown in Figure 3.1. Load was applied to the test specimen by a hydraulic ram via a load cell, swivel head, and spreader beam, as shown in Figure 3.2. The end-plates were subjected to pure moment as the test beam was simply supported and loaded with two equal concentrated loads symmetrically placed. Lateral support for both the test specimen and the spreader beam was provided by lateral brace mechanisms bolted to three steel wide flange frames anchored to the reaction floor of the laboratory.

Each test setup was instrumented with a load cell, three displacement transducers, two gaged calipers, two instrumented bolts, and eighteen strain gages. Data was collected, processed, and recorded with an HP 3497A Data Acquisition/Control Unit and an HP 85 Computer. Real time plots of selected data were made with an HP 7470A Plotter permitting effective monitoring of the test.

The load cell measured the load applied by the

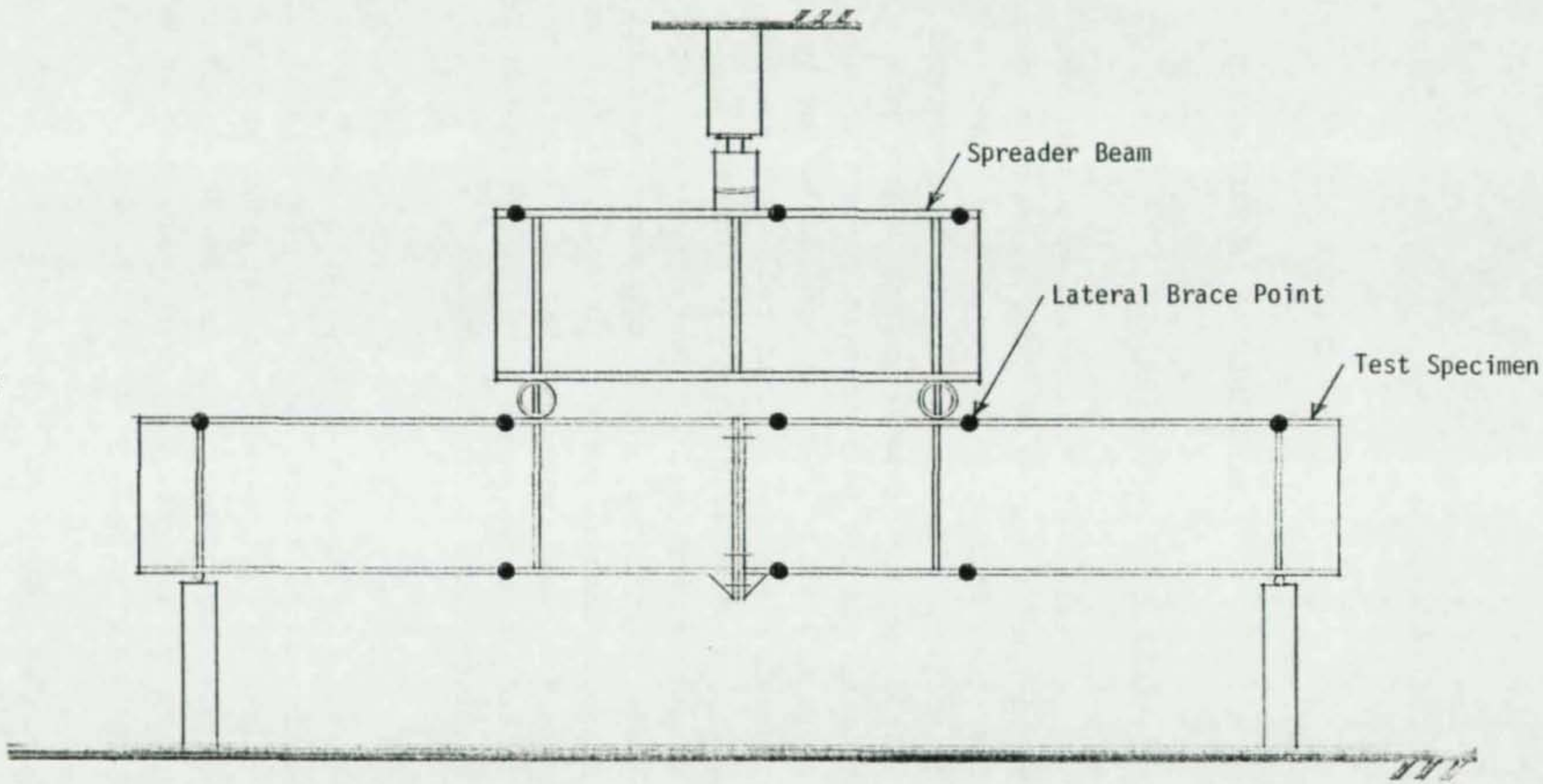

Figure 3.1 Test Setup Longitudinal Elevation

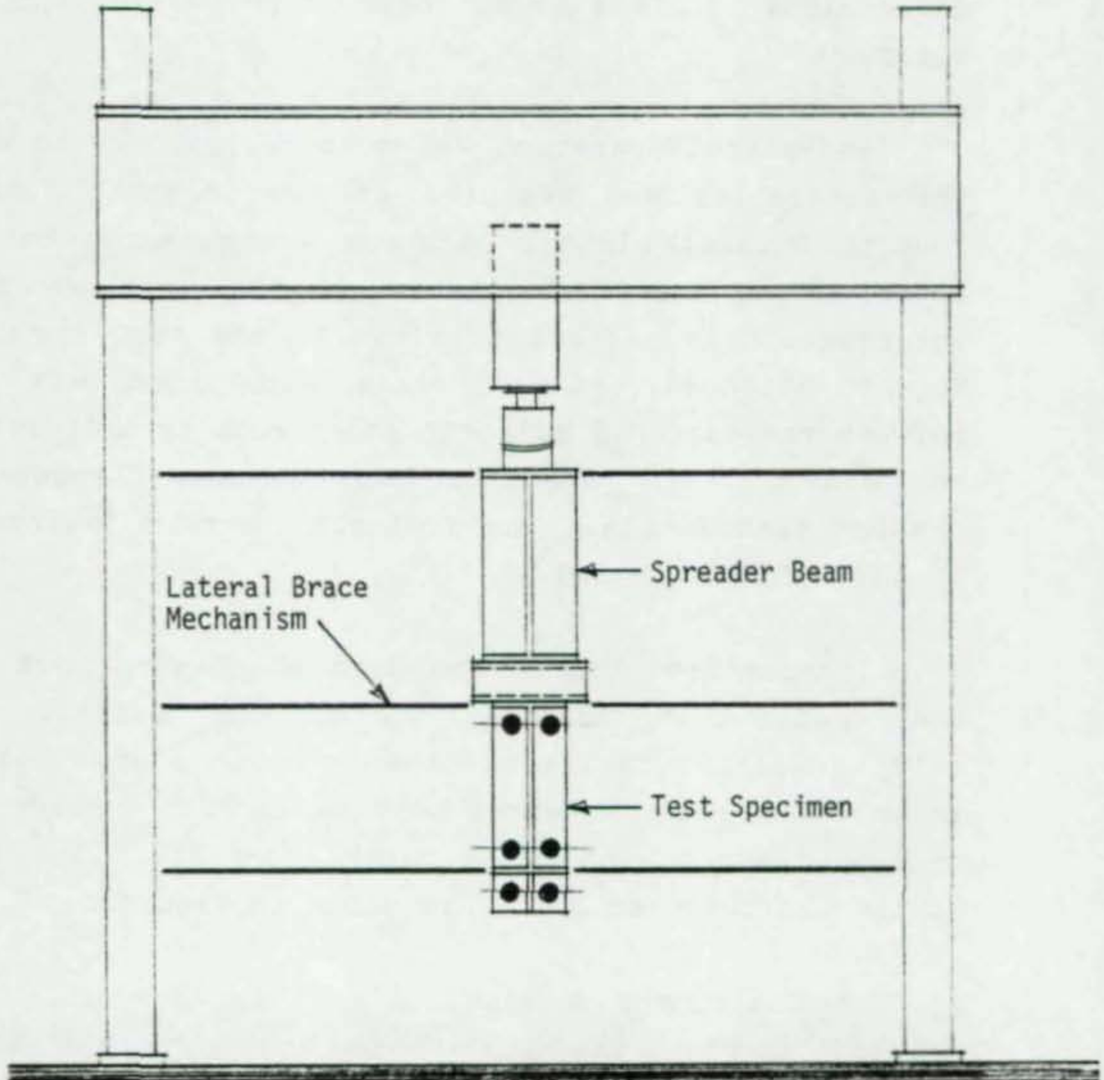

Figure 3.2 Test Setup Transverse Section

hydraulic ram to the test specimen.

Test specimen deflections were measured with displacement transducers. One transducer was located near the test specimen centerline to measure vertical deflection. The two remaining transducers were also located near the test specimen centerline and were used to measure lateral deflections at the test beam compression and tension flanges.

End-plate separation was measured with gaged calipers. The separation was measured at two points: "inner" and "outer". Inner plate separation was measured between the edges of adjacent end-plates at the beam web/end-plate intersection as near as possible to the test specimen beam tension flanges. Outer plate separation was measured between the edges of adjacent end-plates as near as possible to both the test specimen beam tension flanges and the tension flange tips. The location of this instrumentation is shown in Figure 3.3.

Instrumented bolts were used to measure bolt force at two tension bolt locations: "inner" and "outer". An inner bolt is located inside the beam tension flange, within the inner end-plate. An outer bolt is located outside the beam tension flange, within the outer end-plate. The locations of the instrumented bolts are shown in Figure 3.3.

To instrument a bolt, a 3mm diameter hole is first drilled through the bolt head and into the unthreaded portion of the bolt shank. A special strain gage, known as a "bolt gage" is then glued into the hole. The bolt gage is positioned so that its gage length is between the bolt head and the threaded portion of the bolt shank. The bolt is then calibrated using a special fixture in a universal type testing machine. The maximum applied force in the

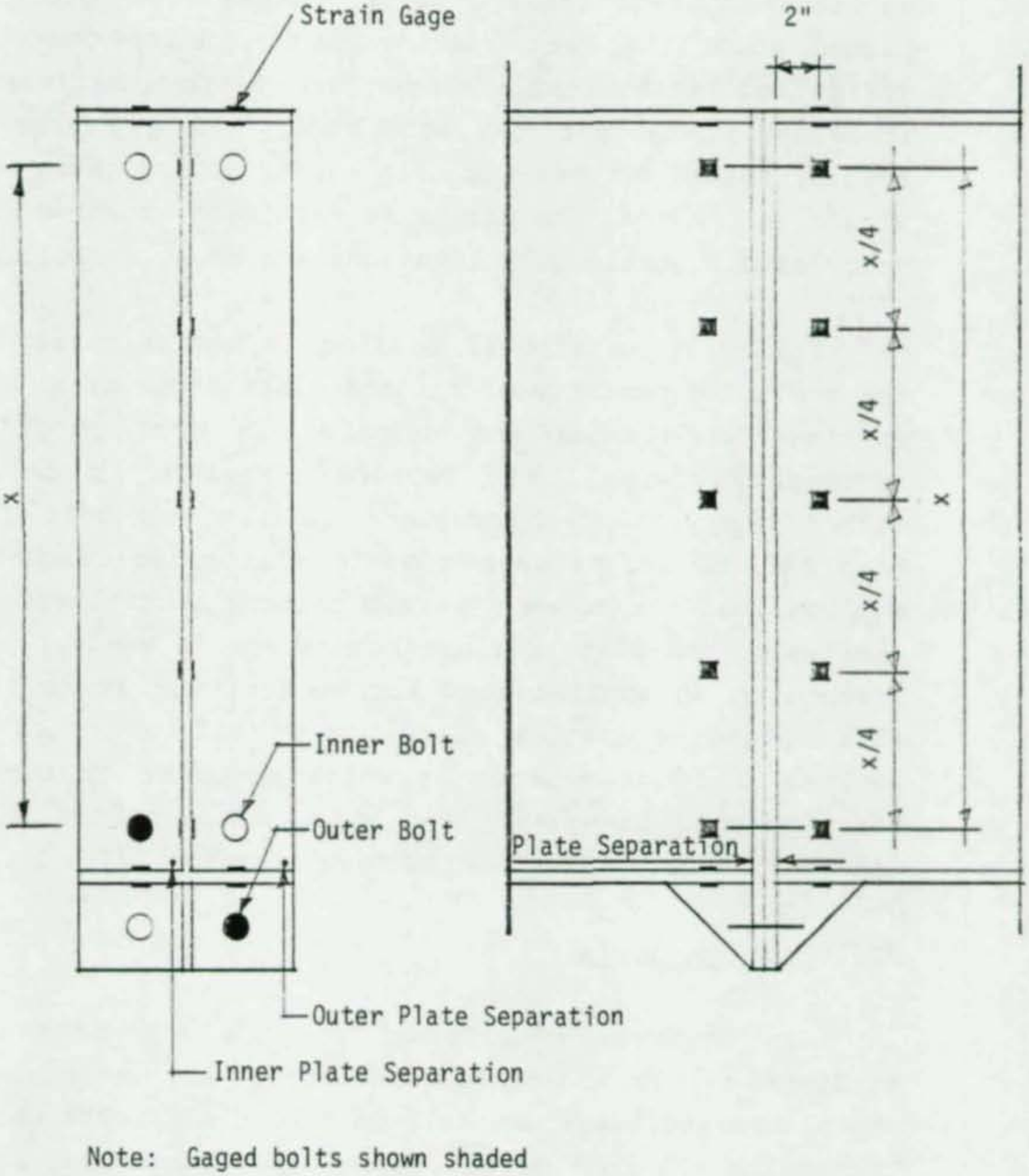

Figure 3.3 Location of Test Specimen Instrumentation

calibration procedure is 90-95% of the bolt proof load.

Eighteen strain gages were located on one of the beam sections adjacent the end-plate. Gages were symmetrically placed about the test specimen web: on the outside and inside of each beam flange and along the beam web, immediately adjacent the bolt holes and at three points equally spaced between the bolt holes. These gages measured strain, and hence, the stress at each gage location could be calculated. Strain gage locations are shown in Figure 3.3.

Following an initial loading to approximately 20% of the predicted capacity of the end-plate connection, the test specimen was loaded and unloaded in four progressively increasing stages until failure. Failure is defined as either beam failure, end-plate failure, or bolt failure. Beam failure occurs when a yield plateau is reached on an applied load (or moment) versus centerline deflection plot. Similarly, end-plate failure occurs when a yield plateau is reached on an applied load (or moment) versus an inner or outer plate separation plot. Bolt failure occurs at the applied load (or moment) at which an inner or outer bolt force reaches its proof load which is twice its allowable tension capacity per the AISC Specification [4].

3.2 Test Specimens

Six tests were performed for the four-bolt extended stiffened moment end-plate connection. All material for the end-plates and beams was A572 Gr 50 and all bolts were A325. To develop the test matrix, geometric parameters, including end-plate thickness and bolt diameter, were varied within limits shown in Table 1.1.

Each test is designated by a specific code, for example, ES-5/8-3/8-16. The ES signifies a four-bolt extended stiffened moment end-plate configuration, 5/8 is the bolt diameter in inches, 3/8 is the nominal end-plate thickness in inches, and 16 represents the nominal beam depth in inches. In summary:

$$\text{ES-5/8-3/8-16 corresponds to ES-}d_b\text{-}t_p\text{-}h \qquad (3.1)$$

The actual geometric parameters for each test were measured and recorded. Table 3.1 summarizes this data.

3.3 Test Results

The results for the six four-bolt extended stiffened moment end-plate tests are presented in Appendices B, C, D, E, F, and G. Each appendix contains a similar presentation of results for an individual test; a Test Synopsis and five plots.

The Test Synopsis sheet summarizes beam, end-plate, and bolt data. Additionally, this sheet presents prediction values and experimental results including the test specimen maximum applied moment and moment at bolt proof load.

The second sheet contains two plots. The first plot is the test setup centerline vertical deflection versus applied end-plate moment. Two curves are plotted: the prediction and the experimental test results. The prediction curve is the strength of materials centerline deflection for a simply supported beam with two equal concentrated loads symmetrically placed:

$$\delta_{pred} = P_{ram} b \,/[48EI\ (3L^2 - 4b^2)] \qquad (3.2)$$

The second plot is end-plate separation versus applied moment. Both the inner and outer end-plate separation curves from the experimental test results are presented.

Table 3.1 Four-Bolt Extended Stiffened Moment End-Plate Parameters

Test Designation	t_p (in)	d_b (in)	P_{ext} (in)	P_f (in)	g (in)	h (in)	b_f (in)	t_w (in)	t_f (in)	F_{py} (ksi)	b (ft)	L (ft)
ES-5/8-3/8-16	0.375	0.625	2.469	1.089	2.734	15.907	6.000	0.227	0.380	55.5	8.063	28.302
ES-3/4-1/2-16	0.481	0.750	3.125	1.120	3.282	15.750	6.000	0.227	0.380	53.2	7.974	28.063
ES-3/4-7/16-20	0.434	0.750	2.625	1.037	2.766	19.938	6.094	0.225	0.479	60.5	10.987	34.057
ES-3/4-1/2-20	0.476	0.750	2.937	1.580	3.500	19.969	6.000	0.225	0.483	51.8	10.984	34.073
ES-1-1/2-24	0.486	1.000	3.218	1.692	3.218	24.063	8.031	0.234	0.496	51.6	15.971	44.047
ES-1-5/8-24	0.620	1.000	2.219	1.723	4.500	23.938	8.000	0.250	0.496	52.7	15.987	44.099

The predicted ultimate moment from a yield-line analysis of the end-plate is also shown on this plot.

The third sheet also contains two plots. Each plot is moment versus bolt force. The first plot contains two curves for the inner bolt: the modified Kennedy method prediction and the experimental test results. The second plot similarly contains two curves for the outer bolt: the modified Kennedy method prediction and the experimental test results. The predicted curves are plotted only for values less than or equal to the bolt proof load. Note that the "bolt force" plotted is a measured change in voltage divided by a calibration factor for a bolt. Since an instrumented bolt is calibrated only in the elastic range, measured "bolt force" is likewise only valid in the elastic range which is less than or equal to the bolt proof load. Actually, the plots represent the change in strain in the bolt shank.

The fourth and final sheet contains a single plot of moment versus rotation or M-Φ diagram. The M-Φ curve is developed by solving the following for the connection rotation, Φ:

$$\delta_{test} = \delta_{pred} + \Phi L/2 \qquad (3.3)$$

δ_{test} is the experimental test specimen centerline deflection and δ_{pred} is the elastic centerline deflection for a simply supported beam with two concentrated loads symmetrically placed, Equation 3.2.

3.4 Supplementary Tests

Standard ASTM E8 18in. tensile test coupons were cut from the same plate used to fabricate the test specimen end-plates. Coupon tests were then performed with a universal testing machine. Results are found in Table 3.2.

Table 3.2

Tensile Coupon Test Results

Coupon	Yield Stress (ksi)	Tensile Stress (ksi)	Elongation (%)
ES-5/8-3/8-16	55.5	76.2	45.5
ES-3/4-1/2-16	53.2	82.1	47.5
ES-3/4-7/16-20	60.5	78.6	45.0
ES-3/4-1/2-20	51.8	81.3	40.5
ES-1-1/2-24	51.6	78.5	46.3
ES-1-5/8-24	52.7	73.5	50.0

CHAPTER IV

COMPARISON OF EXPERIMENTAL TEST RESULTS AND PREDICTIONS

4.1 End-Plate Strength Comparisons

The ultimate moment capacity for each experimental test specimen was calculated using Equation 2.2 or 2.4 as appropriate and the measured yield stress in Table 3.2. The maximum applied moment, predicted ultimate moment, and the ratio of predicted-to-applied moment for each experimental test is shown in Table 4.1. The predicted-to-applied moment ratios varied from 0.71 (conservative) to 1.03 (slightly unconservative). From the moment versus plate separation plots in the appendices, the predicted ultimate moment, except that for Test ES-1-1/2-24, corresponds very closely to the yield plateau of each plate separation curve. In Test ES-1-1/2-24, the maximum applied load significantly exceeded the predicted ultimate load.

4.2 Bolt Force Comparisons

Table 4.1 lists the applied and predicted moments at which bolt proof load was reached in the inner and outer bolts for each experimental test. The bolt proof load is twice the allowable AISC Specification tension capacity. For A325 bolts, the proof load is calculated with 88 ksi and the bolt area based on nominal bolt diameter. Proof loads are 27.0 kips for 5/8 inch diameter bolts, 38.9 kips for 3/4

Table 4.1

Predicted and Experimental Test Results

TEST	End-Plate			Bolt Force					
	Maximum Applied Moment (k-ft)	Predicted Ultimate Moment (k-ft)	Predicted / Applied	Applied Moment at Proof Load		Predicted Moment at Proof Load		Predicted / Applied	
				Inner (k-ft)	Outer (k-ft)	Inner (k-ft)	Outer (k-ft)	Inner	Outer
ES-5/8-3/8-16	114.9	108.4	0.94	97.7	103.8	90.2	93.2	0.92	0.90
ES-3/4-1/2-16	163.4	167.9	1.03	135.8	145.7	135.9	132.9	1.00	0.91
ES-3/4-7/16-20	235.1	208.7	0.89	149.5	165.2	159.1	168.2	1.06	1.02
ES-3/4-1/2-20	203.0	163.3	0.80	149.9	154.1	171.3	168.4	1.14	1.09
ES-1-1/2-24	349.5	249.8	0.71	330.8	N.R.	283.2	361.9	0.86	--
ES-1-5/8-24	379.4	364.5	0.96	301.6	371.6	333.6	360.0	1.11	0.97

N.R. - Bolt proof load not reached in test inch diameter bolts, and 69.1 kips for 1 inch diameter bolts. These values are shown on the moment versus bolt force plots in the appendices.

The predicted moments are obtained by determining values for the factors α and β in Equations 2.8, 2.11, 2.13, and 2.17. These factors proportion the beam tension flange force to the outer and inner end-plates, respectively. The terms, α and β, were empirically determined from the experimental test data as 0.75 and 0.25, respectively, prior to the inner bolts reaching proof load and 0.40 and 0.60, respectively, after the inner bolts had reached proof load.

In all of the experimental tests, the inner bolts reached bolt proof load before the outer bolts. Considering the applied moments at which the inner bolts reached proof load, a $\beta = 0.60$ was selected to best represent the experimental test data. The predicted-to-applied moment ratios for the inner bolt at proof load with $\beta = 0.60$, range from 0.86 to 1.14. The experimental data show that the inner bolt forces, actually strains, increased at an increasing rate after the bolt proof load was reached. This indicates that these inner bolts were not accepting significant additional beam tension flange force.

Considering the applied moments at which the outer bolts reached proof load, an $\alpha = 0.75$ was selected to best represent the experimental test series. The predicted-to-applied moment ratios for the outer bolt at proof load with $\alpha = 0.75$, range from 0.90 to 1.09. Thus most of the additional beam tension flange force, exceeding that necessary to produce the inner bolt force proof load, is taken by the outer bolts. Since the "bolt force" quantity in the moment versus bolt force plots in the appendices is actually bolt strain, once an inner bolt reaches bolt proof

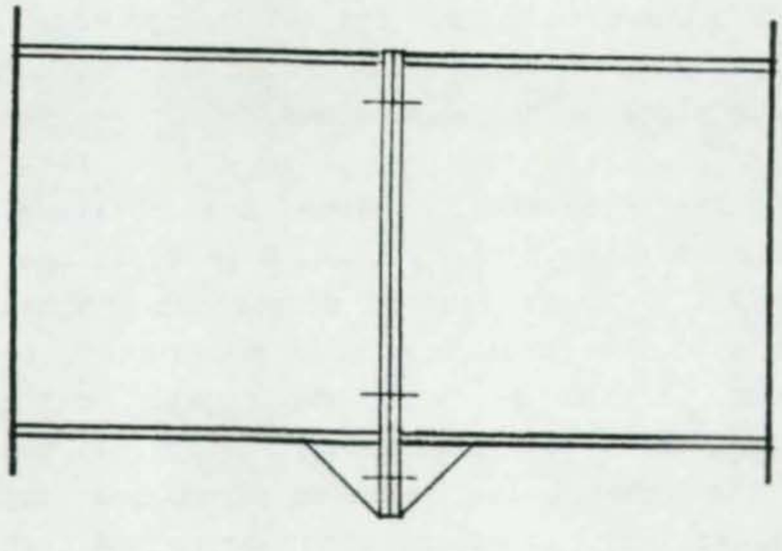

(a) End-Plate Geometry Before Load Application

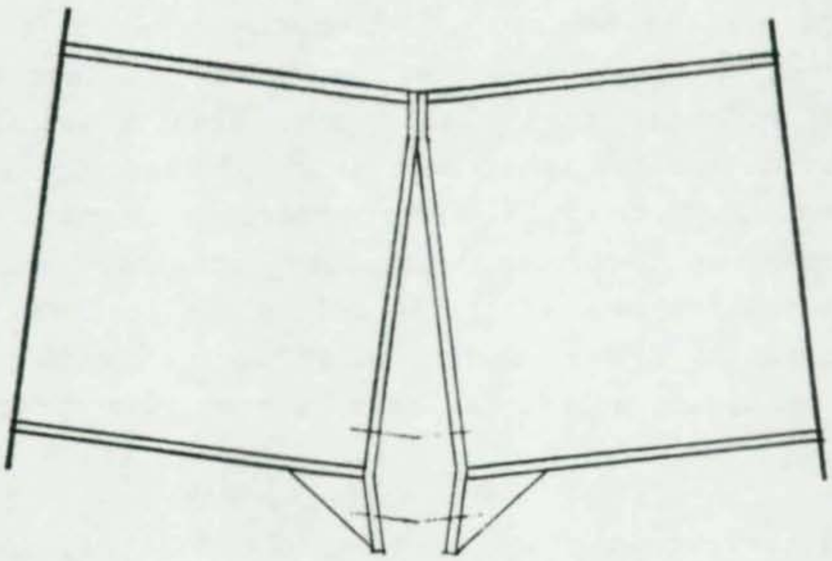

(b) End-Plate Geometry at Increasing Load Levels

Figure 4.1 End-Plate Geometry at the Beam Tension Flange load, yielding begins, and hence, most of the additional beam tension flange force is shed to the outer bolts. The end-plate geometry at the beam tension flange is shown in Figure 4.1.

In summary, the inner bolts always reach bolt proof load before the outer bolts. Further, the inner and outer end-plates, Figure 2.5(b), receive 60% and 40% of the beam tension flange force at maximum moment, respectively.

4.3 Moment-Rotation Comparisons

For the Type I Construction criterion developed in Section 2.3, $0.1\theta_s < 0.00414$ radians and $M_u > 0.9\ M_F$, it is evident from the moment versus rotation plots in the appendices that all of the connections tested are suitable for Type I Construction.

CHAPTER V

DESIGN RECOMMENDATIONS AND EXAMPLE

5.1 Design Recommendations

This study extends the unification of design procedures for moment end-plate connections by Hendrick et al [2] to include a fifth configuration, the four-bolt extended stiffened moment end-plate connection. This unification provides consistent analytical procedures: end-plate strength criterion by yield-line theory and bolt force prediction by a modified Kennedy method. Further, an assessment of the connection rotational stiffness via M-Φ diagrams is presented. These analytical procedures are verified with adequate experimental testing.

The recommended design procedure follows:

1. Compute the factored beam end moment:

$$M_u = M_w/0.6 \tag{5.1}$$

2. Establish values to define the end-plate geometry: b_f, g, p_f, p_t, h, d_e, and t_w.

3. With a known yield stress, F_{py}, determine the required end-plate thickness using the flow chart in Figure 5.1.

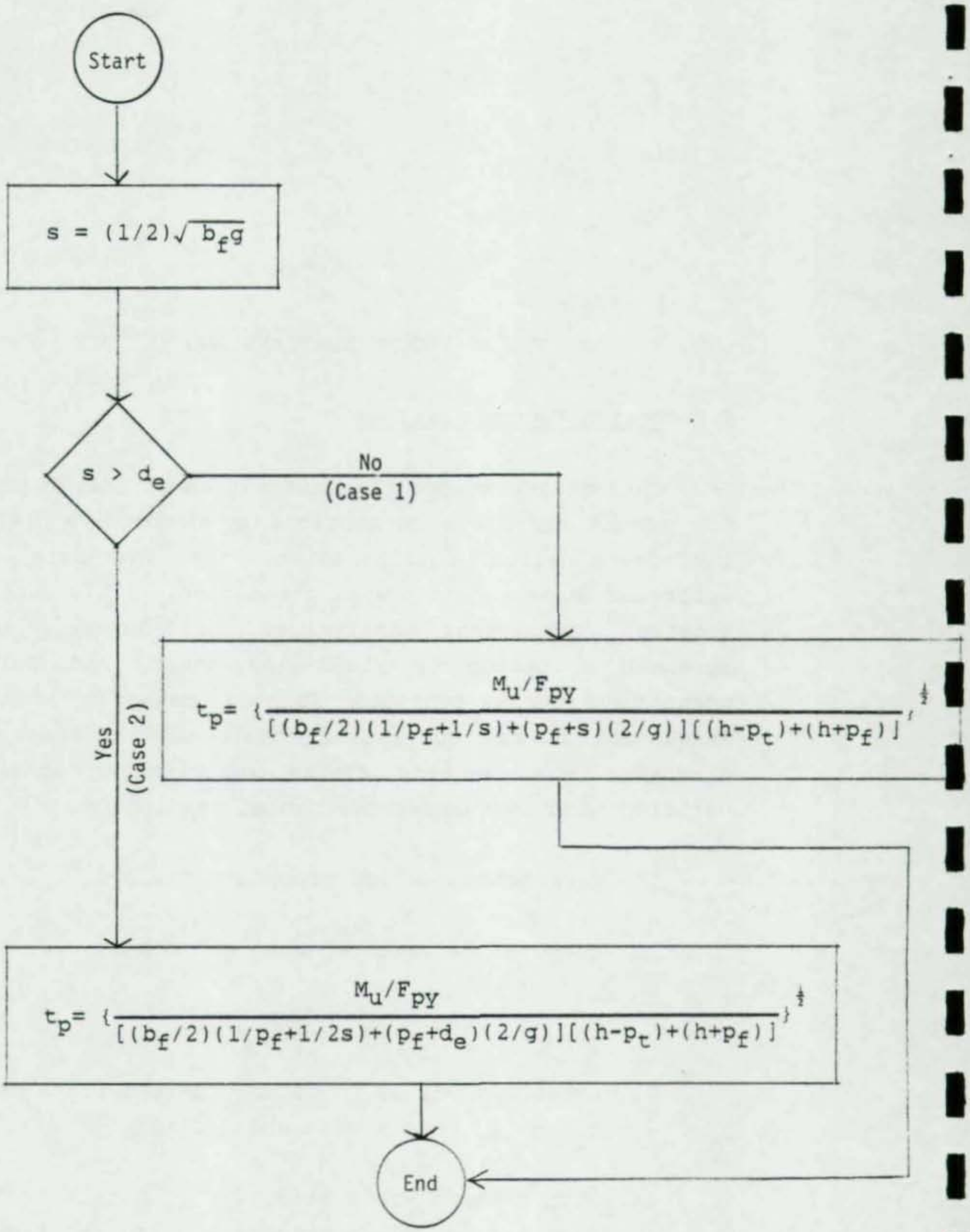

Figure 5.1 Flowchart to Determine End-Plate Thickness

$$\beta = 0.60$$

$$a = 3.682\ (t_p/d_b)^3 - 0.085$$

$$F_f = M_u / (h - t_f)$$

$$F_1 = \frac{b_f t_p^2 F_{py}}{4 p_f \sqrt{1 + (3t_p^2/16p_f^2)}}$$

$$F_{11} = \frac{t_p^2\ F_{py}\ [0.85(b_f/2) + 0.80\ w'] + [(\pi d_b^3 F_{yb})/8]}{2 p_f}$$

$\beta F_f < F_1$

Yes (Thick Plate Behavior): $B_I = \beta F_f / 2$

No

$\beta F_f \le F_{11}$

Yes (Intermediate Plate Behavior):

$$Q = \frac{\beta F_f p_f}{2a} - \frac{\pi d_b^3 F_{yb}}{32a} - \frac{b_f t_p^2}{8a} \sqrt{F_{py}^2 - 3(\beta F_f / b_f t_p)^2}$$

$$B_I = \beta F_f / 2 + Q$$

No (Thin Plate Behavior):

F' = minimum of $F_{limit} = F_{11} / 2$; $F_{max} = \beta F_f / 2$

$$Q_{max} = \frac{w' t_p^2}{4a} \sqrt{F_{py}^2 - 3(F'/w' t_p)^2}$$

$$B_I = \beta F_f / 2 + Q_{max}$$

Figure 5.2 Flowchart to Determine Inner (Controlling) Bolt Force

4. Select a trial bolt diameter and compute the inner (controlling) bolt force using the flowchart in Figure 5.2.

5. The required bolt diameter is determined from:

$$d_b = \sqrt{2B_I/\pi F_a} \tag{5.2}$$

where F_a = the allowable stress for the bolt material.

In the AISC Specification [4], the allowable tensile stress for A325 bolt material is 44 ksi with a factor of safety against yielding of 2.0. Equation 5.2 reflects this factor of safety.

Geometric limitations for the design procedure are found in Table 1.1. The procedure is demonstrated in Section 5.2.

5.2 Design Example

Determine the required end-plate thickness and bolt size for a four-bolt extended stiffened moment end-plate connection given the following:

Beam data...

A572 Gr 50 steel	F_y = 50 ksi
Depth of beam	h = 24 in
Flange width	b_f = 8 in
Web thickness	t_w = 1/4 in
Flange thickness	t_f = 1/2 in

End-plate data...

A572 Gr 50 material	F_{yp} = 50 ksi
Extension outside beam flange	p_{ext} = 3-1/4 in
Pitch to bolt from beam flange	p_f = 1-5/8 in
Gage	g = 3-1/4 in

Bolt data...

A325 $F_a = 44$ ksi

Other data...

Working moment $M_w = 125$ k-ft

Construction Type — Type *I*

<u>Step 1.</u> Determine M_u.

$$M_u = M_w/0.60$$

$$= 105/0.60 = 175.0 \text{ k-ft.}$$

<u>Step 2.</u> Determine s and required end-plate thickness.

$$s = (1/2)\sqrt{b_f g}$$

$$= (1/2)\sqrt{8(3.25)} = 2.55 \text{ in.}$$

Since s = 2.55 in. > d_e = 1-5/8 in. Case 2 applies.

$$t_p = \left\{\frac{M_u/F_{py}}{[(b_f/2)(1/p_f+0.5/s)+(p_f+d_e)(2/g)][(h-p_t)+(h+p_f)]}\right\}^{\frac{1}{2}}$$

$$= \left\{\frac{175.0(12)/50}{[(8/2)(1/1.625+0.5/2.55)+(1.625+1.625)(2/3.25)]\,[(24-2.125)+(24+1.625)]}\right\}^{\frac{1}{2}}$$

$$= 0.411 \text{ in.} \quad \text{Try } t_p = 7/16 \text{ in.}$$

<u>Step 3.</u> Determine flange force.

$$F_f = M_u/(h-t_f)$$
$$= [175.0(12)]/(24-0.5) = 89.4 \text{ kips}$$

<u>Step 4.</u> Determine inner end-plate behavior.

$$F_1 = \frac{b_f t_p^2 F_{py}}{4p_f\sqrt{1+(3t_p^2/16p_f^2)}}$$

$$= \frac{8(0.438)^2(50)}{4(1.625)\sqrt{1+[3(0.438)^2/16(1.625)^2]}} = 11.7 \text{ kips}$$

Try 1 in. diameter bolts.

$$w' = (b_f/2)-[d_b+(1/16)]$$

$$= (8/2)-(1+0.0625) = 2.94 \text{ in.}$$

$$F_{11} = \frac{t_p^2F_{py}[0.85(b_f/2)+0.80w']+[(\pi d_b^3F_{yb})/8]}{2p_f}$$

$$= \frac{(0.438)^2 50[0.85(8/2)+0.80(2.94)]+[\pi(1)^3(88)/8]}{2(1.625)}$$

$$= 27.6 \text{ kips}$$

Since $\beta F_f = 0.60(89.4) = 53.6$ kips $> F_{11} = 27.6$ kips, inner end-plate behavior is thin plate behavior.

Step 5. Determine inner bolt force.

$$a = 3.682(t_p/d_b)^3 - 0.085$$

$$= 3.682(0.438/1)^3 - 0.085 = 0.224 \text{ in.}$$

$$F' = \min \left| \begin{array}{l} F_{limit} = F_{11}/2 = 27.6/2 = 13.8 \text{ kips} \\ F_{max} = \beta F_f/2 = 0.60(89.4)/2 = 26.8 \text{ kips} \end{array} \right.$$

$$= 13.8 \text{ kips}$$

$$Q_{max} = \frac{w' t_p^2}{4a} \sqrt{F_{py}^2 - 3(F'/w' t_p)^2}$$

$$= \frac{2.94(0.438)^2}{4(0.224)} \sqrt{(50)^2 - 3[13.8/2.94(0.438)]^2}$$

$$= 29.2 \text{ kips}$$

$$B_I = BF_f/2 + Q_{max}$$

$$= 0.60(89.4)/2 + 29.2 = 56.0 \text{ kips}$$

Step 6. Determine bolt diameter.

$$d_b = \sqrt{2B_I/\pi F_a}$$

$$= \sqrt{2(56.0)/[\pi(44)]}$$

$$= 0.900 \text{ in.} \qquad \text{Use } d_b = 1 \text{ in.}$$

Note: Required bolt diameter is the same as assumed; therefore, no iteration is necessary.

Summary. For materials, geometry, and given loading use A572 Gr 50 end-plate with 7/16 in. thickness and 1 in. diameter A325 bolts.

REFERENCES

1. Srouji, R., Kukreti, A., and Murray, T., "Yield-Line Analysis of End-Plate Connections with Bolt Force Predictions", Fears Structural Engineering Laboratory Report No. FSEL/MBMA 83-05, University of Oklahoma, Norman, Oklahoma, December 1983.

2. Hendrick, D., Kukreti, A., and Murray, T., "Unification of Flush End-Plate Design Procedures", Fears Structural Engineering Laboratory Report No. FSEL/MBMA 85-01, University of Oklahoma, Norman, Oklahoma, March 1985.

3. Kennedy, N.A., Vinnakota, S., and Sherbourne, A.N., "The Split-Tee Analogy in Bolted Splices and Beam-Column Connections", Joints in Structural Steelwork, Proceedings of the International Conference on Joints in Steelwork, held at Middlesbrough, Cleveland, John Wiley and Sons, New York - Toronto, 1981, pp. 2.138-2.157.

4. "Specification for the Design, Fabrication and Erection of Structural Steel for Buildings", American Institute of Steel Construction, New York, 1978.

5. Manual of Steel Construction, 8th ed., American Institute of Steel Construction, Chicago, Illinois, 1980.

6. Salmon, C.G. and Johnson, V.E., Steel Structures Design and Behavior, 2nd ed., Harper and Row, New York, 1980, pp. 729-733.

7. McGuire, W., Steel Structures, Prentice-Hall, Englewood Cliffs, New Jersey, 1968, pp. 890-914.

APPENDIX A

NOMENCLATURE

NOMENCLATURE

a	= distance from bolt centerline to prying force for plate
B	= bolt force
B_I	= inner bolt force
B_o	= outer bolt force
b	= distance from concentrated load to support for test specimen
b_f	= beam flange width
d_b	= bolt diameter
d_e	= distance from bolt centerline to edge of end-plate extension
E	= Young's modulus of elasticity
ES	= extended stiffened
F	= force
F_a	= bolt material allowable stress
F_f	= flange force
	= M_u / $(h - t_f)$
F_{limit}	= possible flange force per bolt at the thin plate limit
F_{max}	= possible flange force per bolt at the thin plate limit
F_{py}	= plate material yield stress
F_y	= yield stress
F_{yb}	= bolt material yield stress
	= bolt proof which is twice the allowable tension capacity per AISC Specification
F'	= flange force per bolt at the thin plate limit
F_1	= flange force at the thick plate limit
F_{11}	= flange force at the thin plate limit

g = end-plate bolt gage

h = beam depth

I = beam moment of inertia

L = distance between test specimen supports

M = moment

M_b = bolt moment capacity when bolt force is at bolt proof which is twice the allowable tension capacity per AISC Specification

M_F = fixed end moment; yield moment

M_u = end-plate ultimate moment capacity

M_{yb} = bolt moment capacity when bolt force is at bolt proof which is twice the allowable tension capacity per AISC Specification

M_w = working moment

M_1 = plastic moment at first hinge line to form

M_2 = plastic moment at second hinge line to form

m_p = plastic moment capacity of plate per unit length
$= (F_{py}\ t_p^2)\ /\ 4$

P_{ram} = load applied to test specimen by hydraulic ram

p_{ext} = end-plate extension outside beam flange
$= p_f + d_e$

p_f = distance from bolt centerline to near face of beam flange

p_t = distance from bolt centerline to far face of beam flange
$= p_f + t_f$

Q = prying force

Q_{max} = maximum prying force

S = section modulus

s = distance from bolt centerline to outermost yield-line

t_f = beam flange thickness

t_p = end-plate thickness

t_w = beam web thickness; stiffener thickness

t_1 = plate thickness at thick plate limit

t_{11} = plate thickness at thin plate limit

w'	= end-plate width per bolt less bolt hole diameter (at bolt line).
x	= distance
α	= outer end-plate factor
β	= inner end-plate factor
δ_{pred}	= predicted strength of materials centerline deflection for test specimen
δ_{test}	= experimental test centerline deflection for test specimen
θ_s	= simple span end rotation for any loading
π	= pi
Φ	= rotation

APPENDIX B

ES-5/8-3/8-16 TEST RESULTS

TEST SYNOPSIS

PROJECT:	MBMA END-PLATE			
TEST:	ES-5/8-3/8-16			
TEST DATE:	6-28-85			
CONNECTION DESCRIPTION:	Four-bolt extended stiffened moment end-plate with single row of two bolts each side of beam tension flange			
BEAM DATA:				
Depth	h	(in)	=	15.907
Flange width	bf	(in)	=	6.0
Web thickness	tw	(in)	=	0.227
Flange thickness	tf	(in)	=	0.380
Moment of inertia	I	(in**4)	=	340.6
END-PLATE DATA:				
Thickness	tp	(in)	=	0.375
Extension outside beam flange	Pext	(in)	=	2.469
Pitch to bolt from flange	Pf	(in)	=	1.089
Gage	g	(in)	=	2.734
Steel yield stress (measured)	Fpy	(ksi)	=	55.5
BOLT DATA:				
Type			=	A325
Diameter	db	(in)	=	0.625
Pretension force	Tb	(k)	=	19.0
PREDICTION:				
End-plate failure moment	Mu	(k-ft)	=	108.4
Bolt failure (proof) moment	Myb	(k-ft)	=	90.2
Beam failure moment		(k-ft)	=	198.5
EXPERIMENTAL:				
Maximum applied moment		(k-ft)	=	114.9
Moment at bolt proof load		(k-ft)	=	97.7
Maximum vertical centerline deflection		(in)	=	2.156
Maximum inner end-plate separation		(in)	=	0.05522
Maximum outer end-plate separation		(in)	=	0.03601

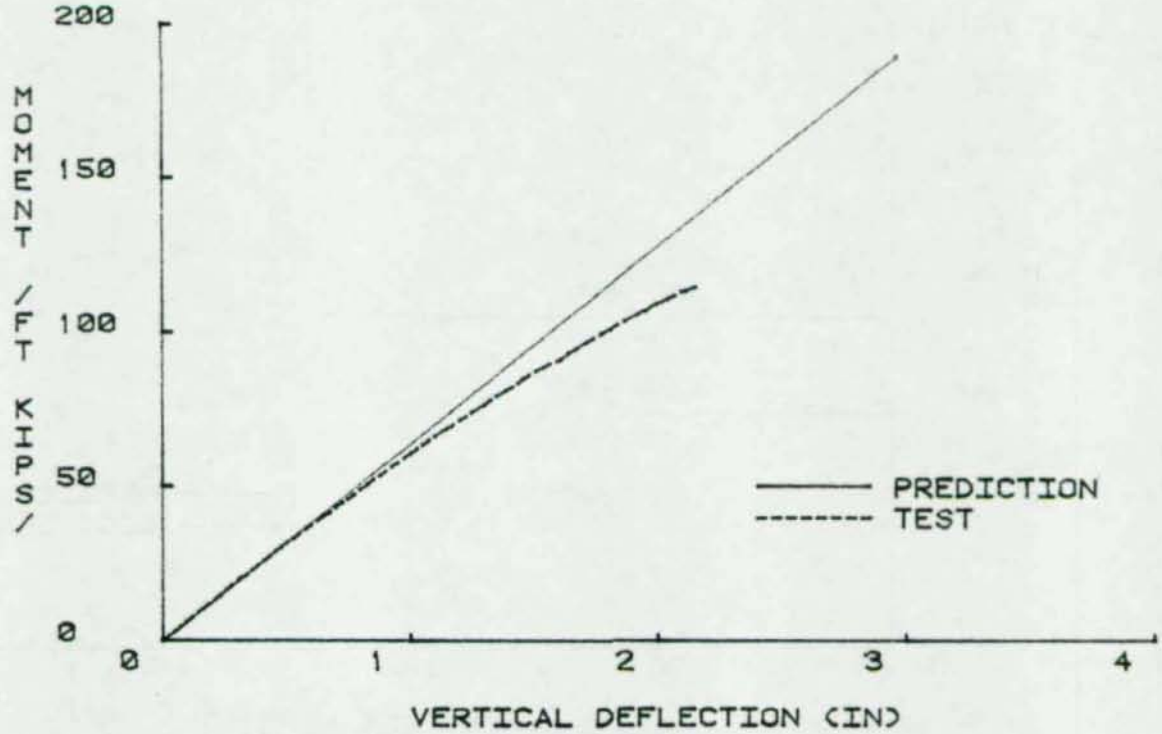

(a) End-Plate Moment versus Midspan Deflection

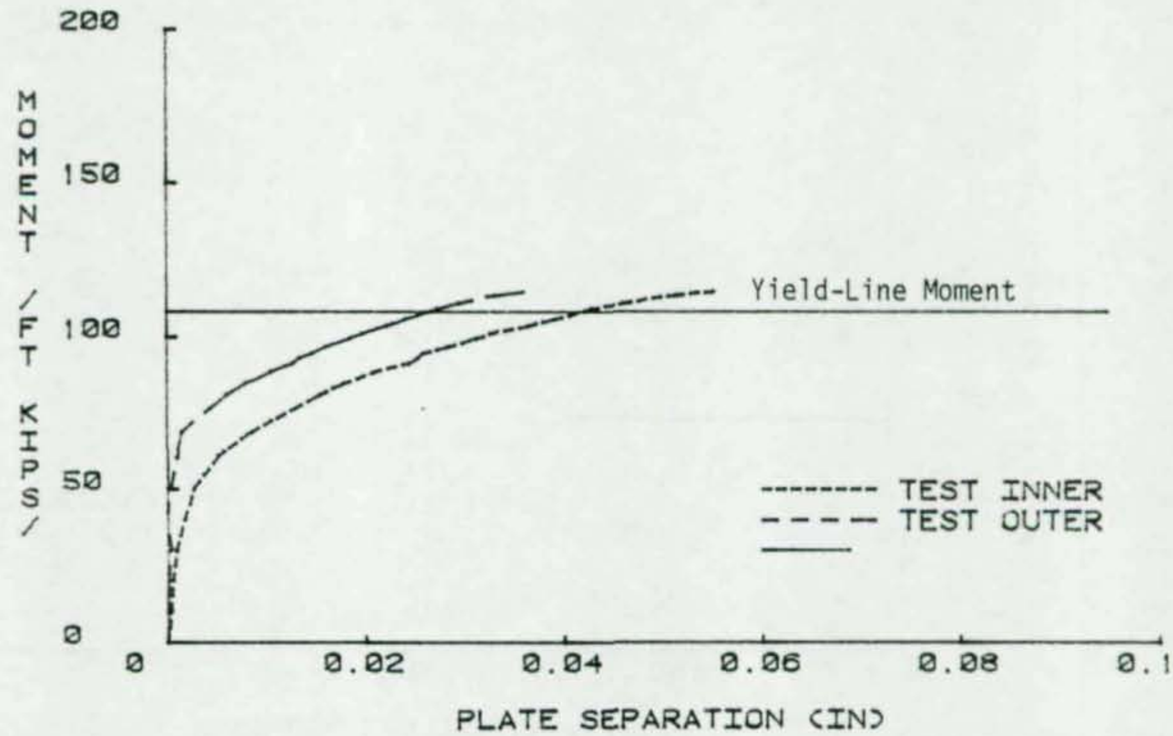

(b) End-Plate Moment versus Plate Separation

Figure B.1 Results from Test ES-5/8-3/8-16

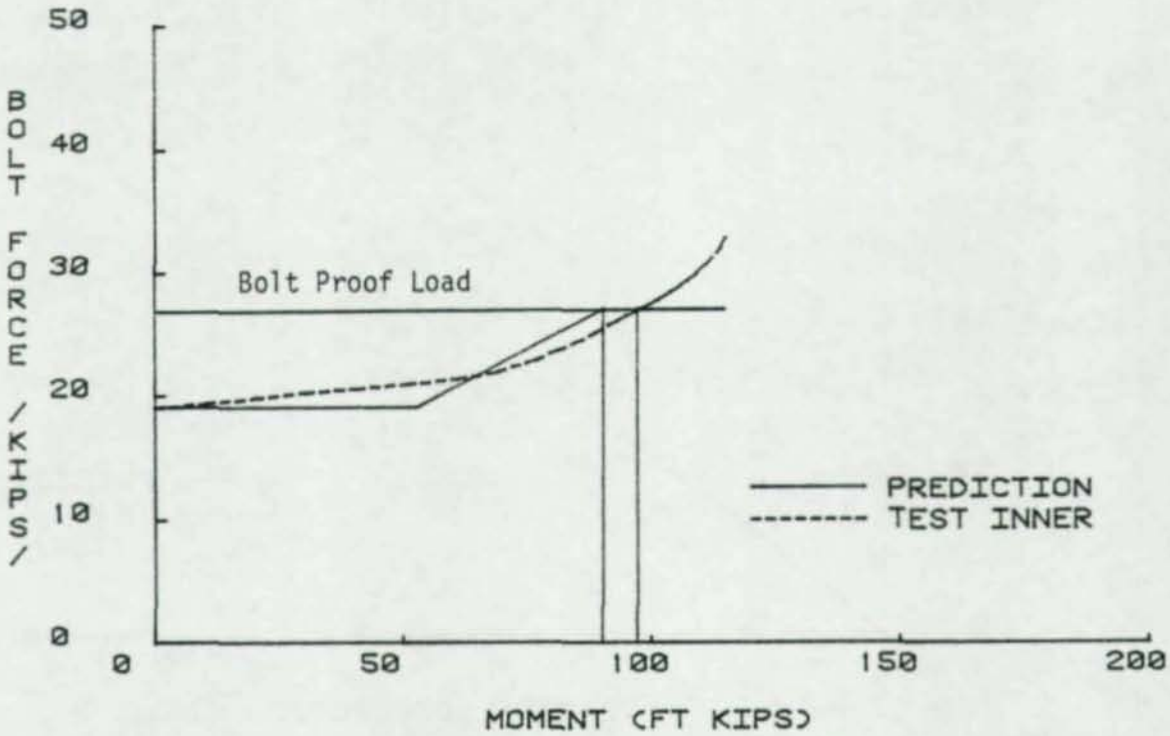

(c) Inner Bolt Force versus End-Plate Moment

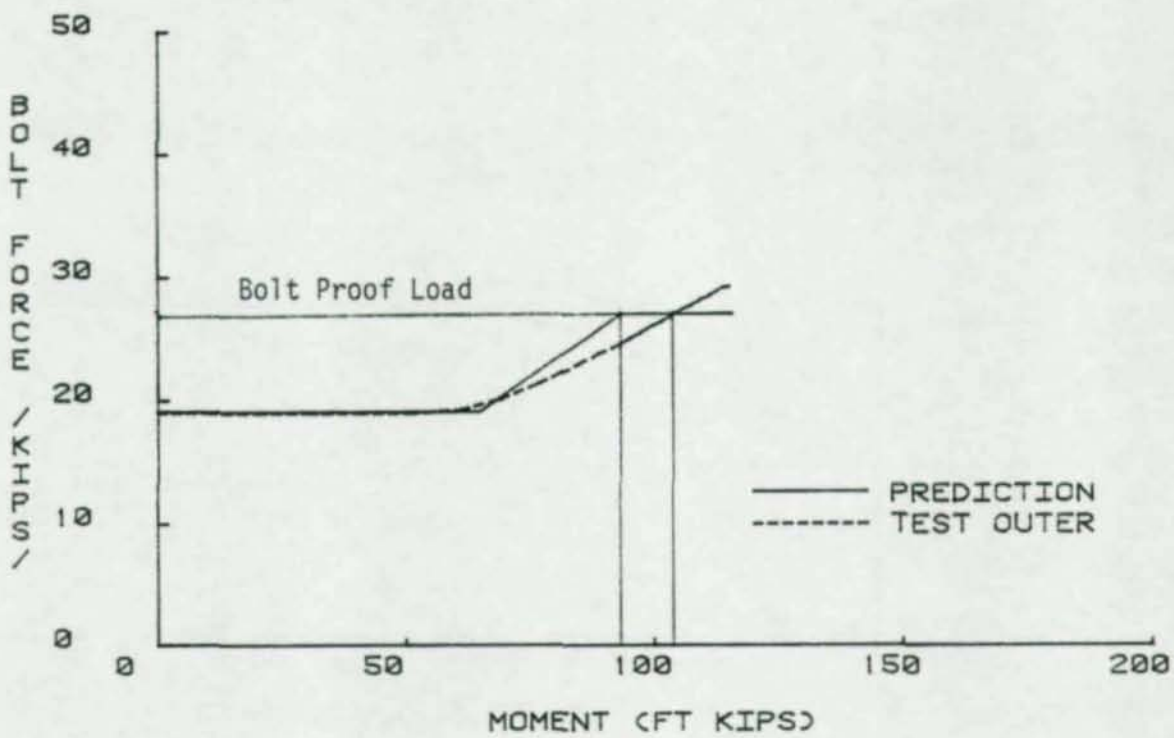

(d) Outer Bolt Force versus End-Plate Moment

Figure B.1 Results from Test ES-5/8-3/8-16, Continued

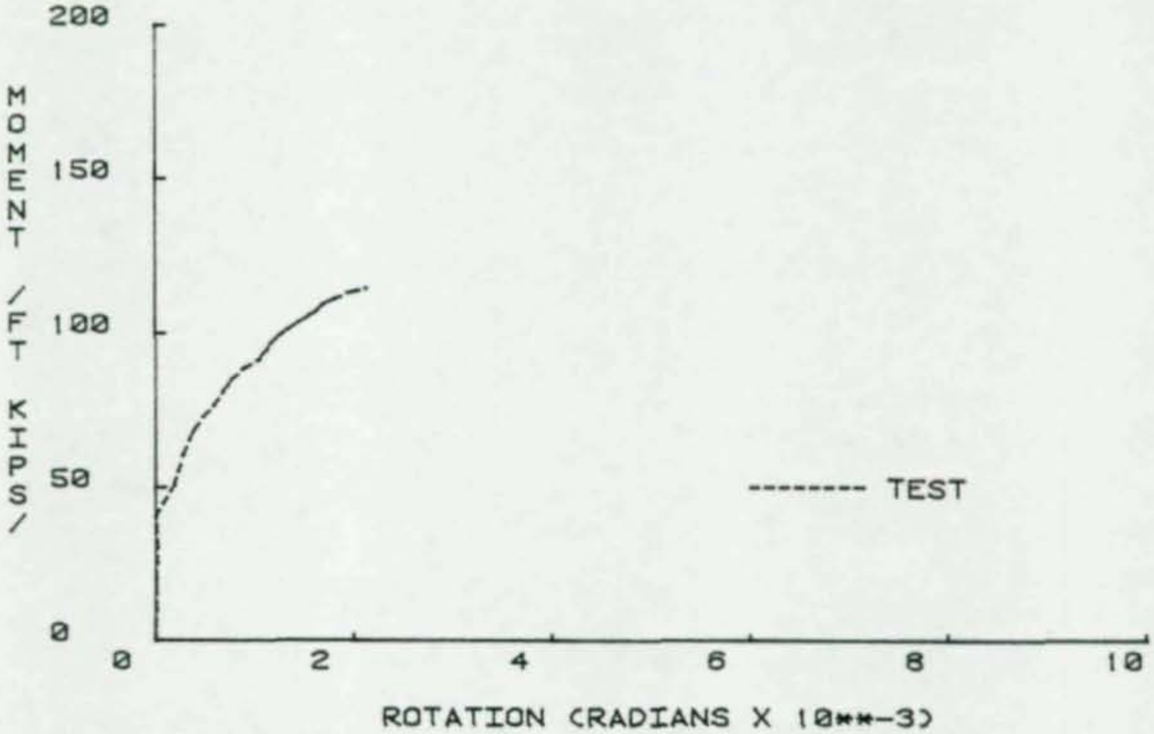

(e) End-Plate Moment versus Rotation

Figure B.1 Results from Test ES-5/8-3/8-16, Continued

APPENDIX C

ES-3/4-1/2-16 TEST RESULTS

TEST SYNOPSIS

PROJECT:	MBMA END-PLATE			
TEST:	ES-3/4-1/2-16			
TEST DATE:	7-10-85			
CONNECTION DESCRIPTION:	Four-bolt extended stiffened moment end-plate with a single row of two bolts each side of beam tension flange			
BEAM DATA:				
Depth	h	(in)	=	15.750
Flange width	bf	(in)	=	6.0
Web thickness	tw	(in)	=	0.227
Flange thickness	tf	(in)	=	0.380
Moment of inertia	I	(in**4)	=	333.1
END-PLATE DATA:				
Thickness	tp	(in)	=	0.481
Extension outside beam flange	Pext	(in)	=	3.125
Pitch to bolt from flange	Pf	(in)	=	1.120
Gage	g	(in)	=	3.282
Steel yield stress (measured)	Fpy	(ksi)	=	53.2
BOLT DATA:				
Type			=	A325
Diameter	db	(in)	=	0.750
Pretension force	Tb	(k)	=	28.0
PREDICTION:				
End-plate failure moment	Mu	(k-ft)	=	167.9
Bolt failure (proof) moment	Myb	(k-ft)	=	132.9
Beam failure moment		(k-ft)	=	187.9
EXPERIMENTAL:				
Maximum applied moment		(k-ft)	=	163.4
Moment at bolt proof load		(k-ft)	=	135.8
Maximum vertical centerline deflection		(in)	=	3.299
Maximum inner end-plate separation		(in)	=	0.09240
Maximum outer end-plate separation		(in)	=	0.08009

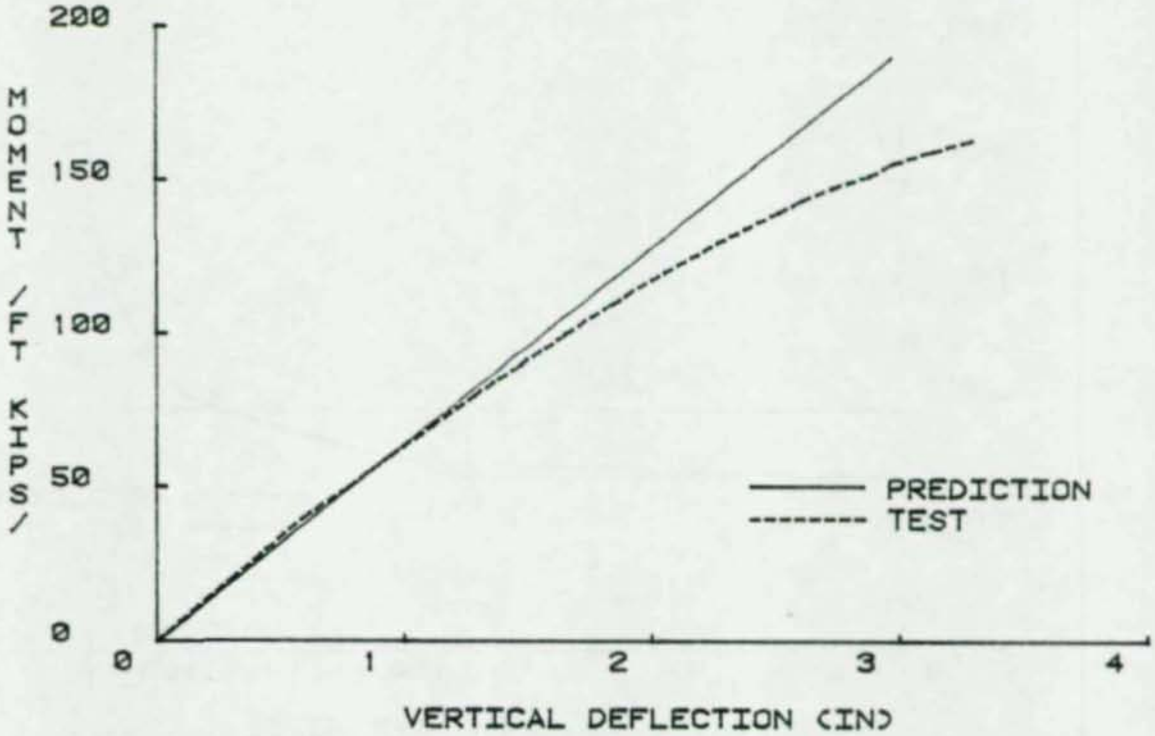

(a) End-Plate Moment versus Midspan Deflection

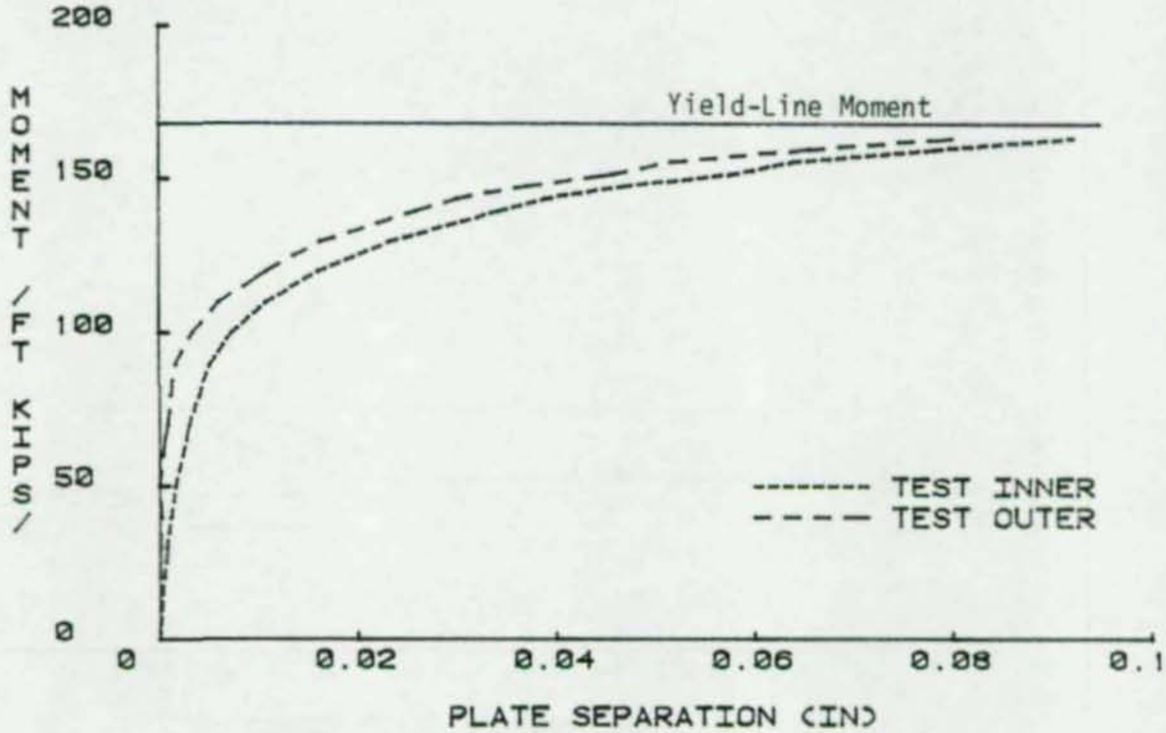

(b) End-Plate Moment versus Plate Separation

Figure C.1 Results from Test ES-3/4-1/2-16

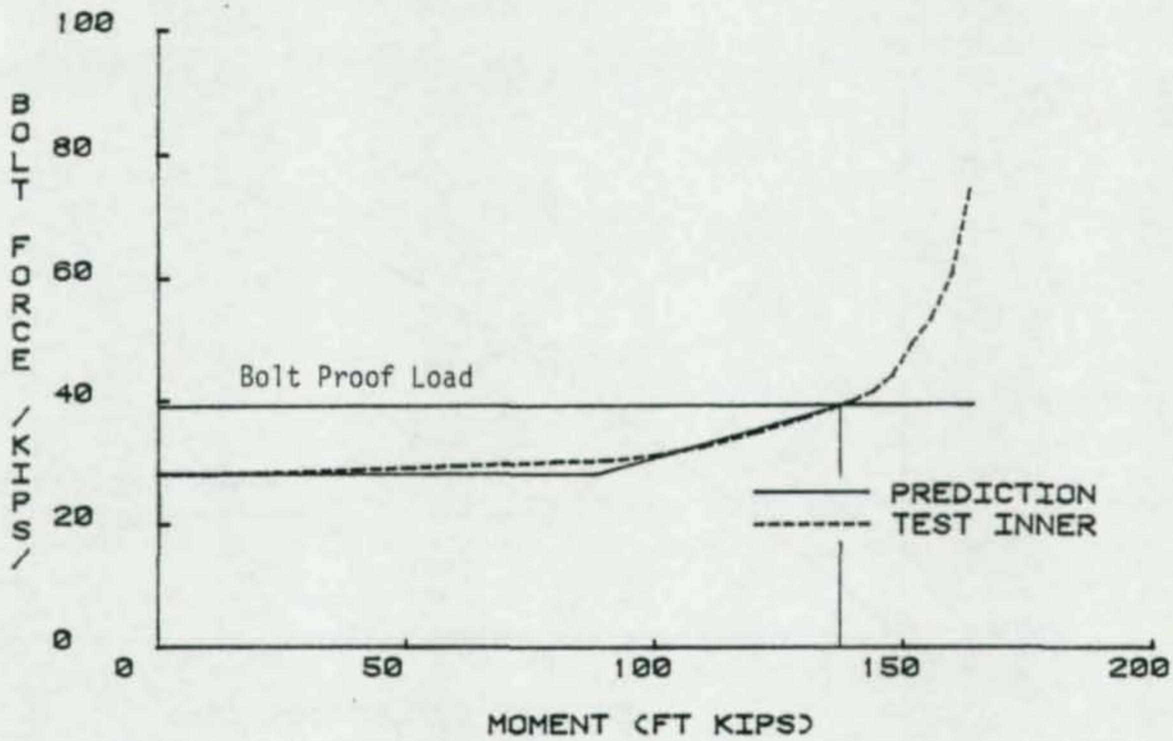

(c) Inner Bolt Force versus End-Plate Moment

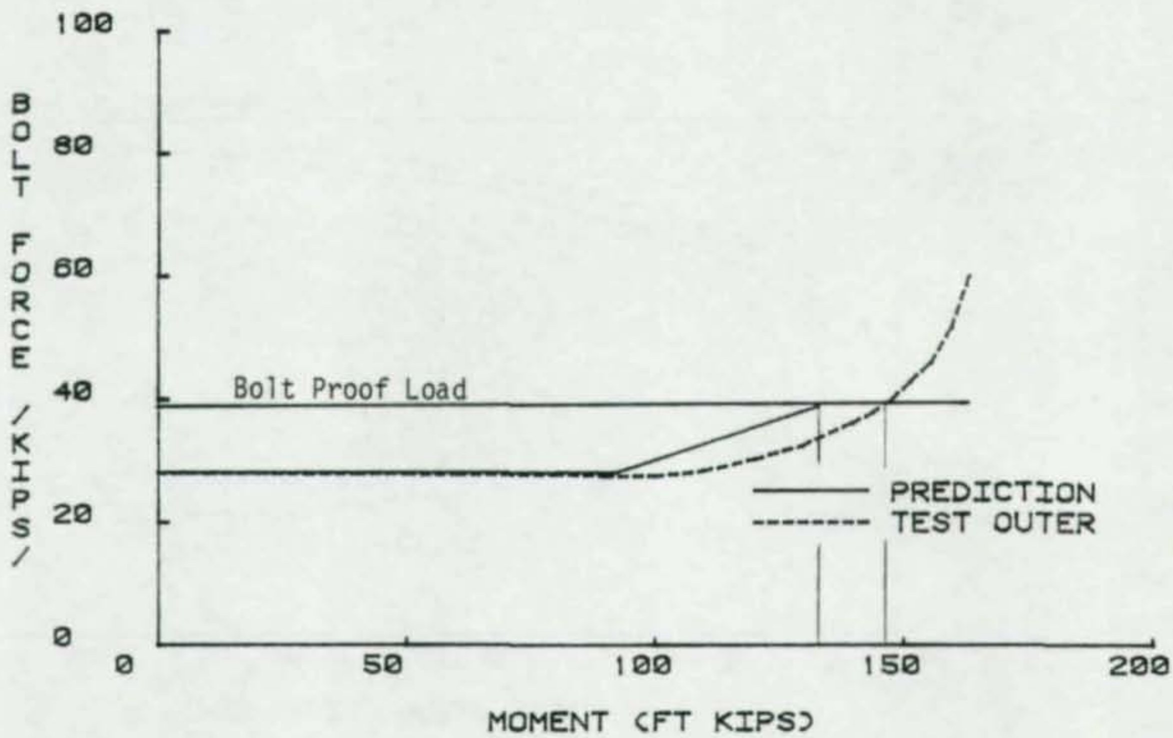

(d) Outer Bolt Force versus End-Plate Moment

Figure C.1 Results from Test ES-3/4-1/2-16, Continued

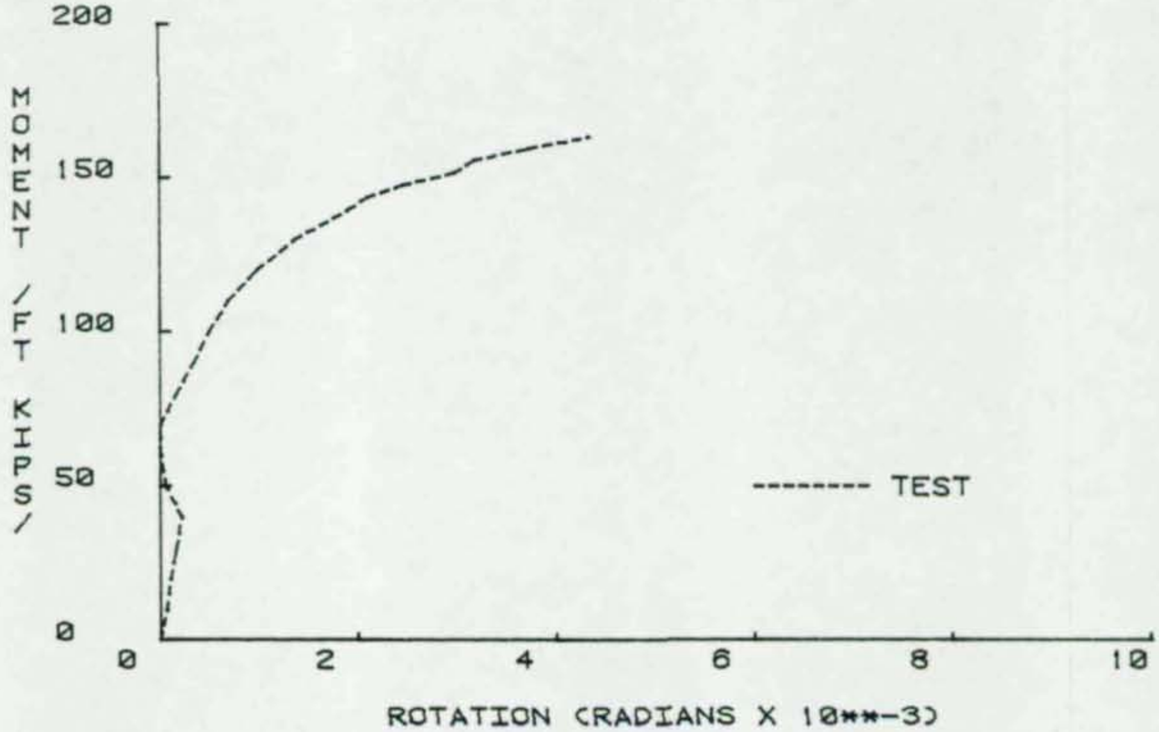

(e) End-Plate Moment versus Rotation

Figure C.1 Results from Test ES-3/4-1/2-16, Continued

APPENDIX D

ES-3/4-7/16-20 TEST RESULTS

TEST SYNOPSIS

PROJECT:	MBMA END-PLATE
TEST:	ES-3/4-7/16-20
TEST DATE:	7-23-85
CONNECTION DESCRIPTION:	Four-bolt extended stiffened moment end-plate with a single row of two bolts each side of beam tension flange

BEAM DATA:				
Depth	h	(in)	=	19.938
Flange width	bf	(in)	=	6.094
Web thickness	tw	(in)		0.225
Flange thickness	tf	(in)	=	0.479
Moment of inertia	I	(in**4)	=	681.0
END-PLATE DATA:				
Thickness	tp	(in)	=	0.434
Extension outside beam flange	Pext	(in)	=	2.625
Pitch to bolt from flange	Pf	(in)	=	1.037
Gage	g	(in)	=	2.766
Steel yield stress (measured)	Fpy	(ksi)	=	60.5
BOLT DATA:				
Type			=	A325
Diameter	db	(in)	=	0.750
Pretension force	Tb	(k)	=	28.0
PREDICTION:				
End-plate failure moment	Mu	(k-ft)	=	208.7
Bolt failure (proof) moment	Myb	(k-ft)	=	159.1
Beam failure moment		(k-ft)	=	345.1
EXPERIMENTAL:				
Maximum applied moment		(k-ft)	=	235.1
Moment at bolt proof load		(k-ft)	=	149.5
Maximum vertical centerline deflection		(in)	=	3.416
Maximum inner end-plate separation		(in)	=	0.09256
Maximum outer end-plate separation		(in)	=	0.03139

DISCUSSION:

An instrumentation problem occurred with the caliper measuring outer end-plate separation. The maximum outer end-plate separation reported is smaller than that anticipated.

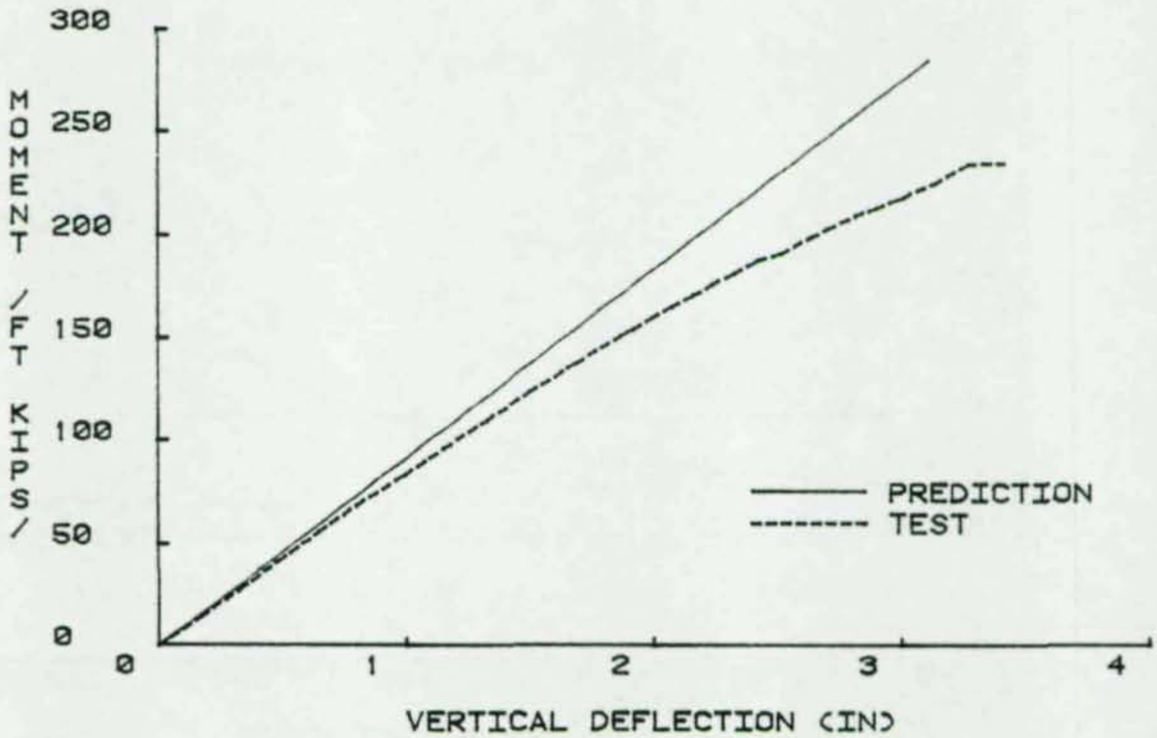

(a) End-Plate Moment versus Midspan Deflection

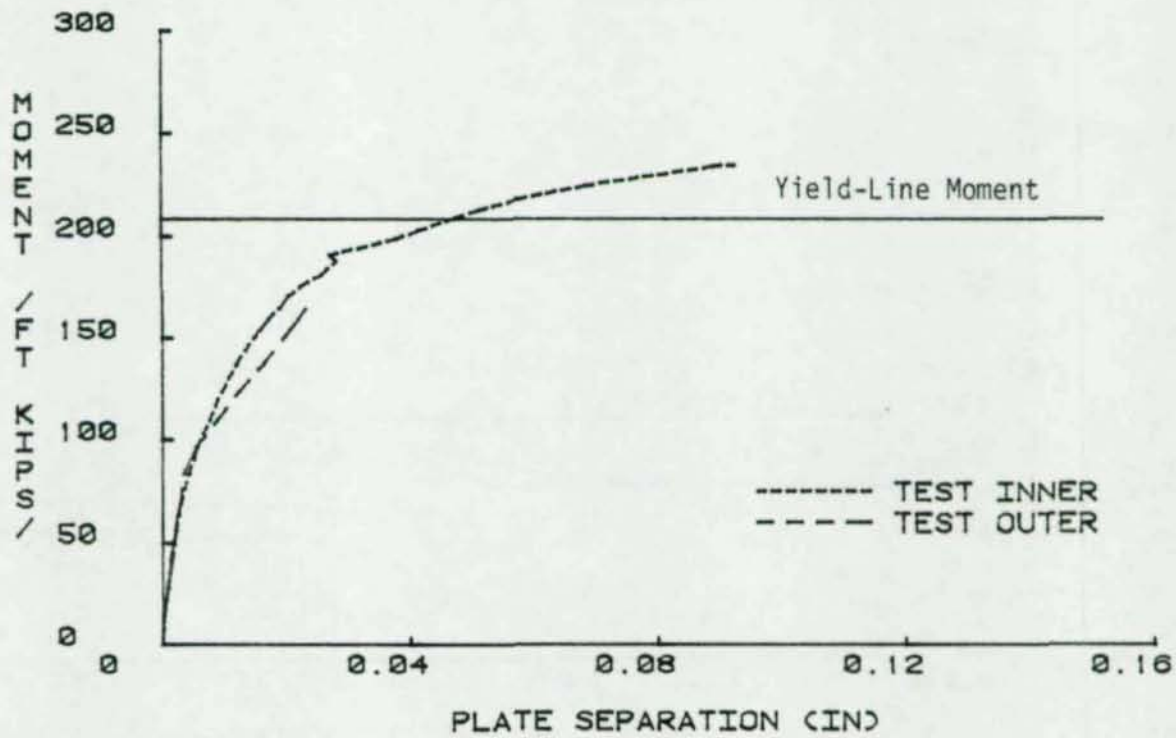

(b) End-Plate Moment versus Plate Separation

Figure D.1 Results from Test ES-3/4-7/16-20

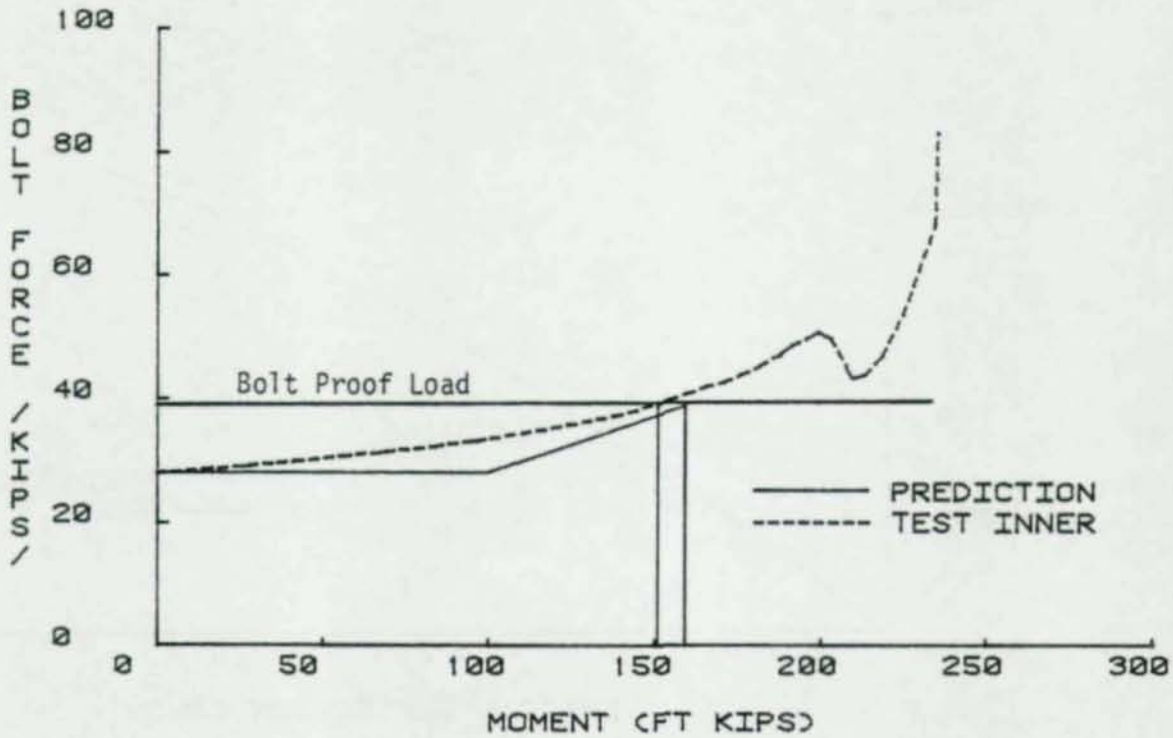

(c) Inner Bolt Force versus End-Plate Moment

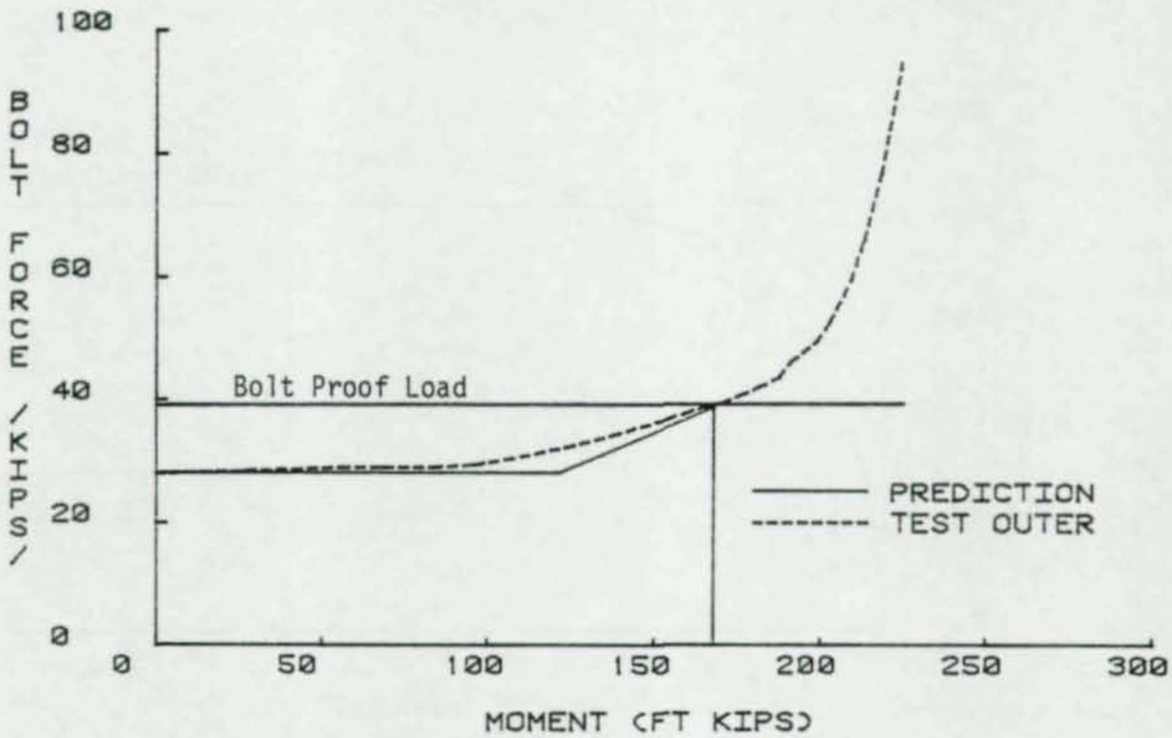

(d) Outer Bolt Force versus End-Plate Moment

Figure D.1 Results from Test ES-3/4-7/16-20, Continued

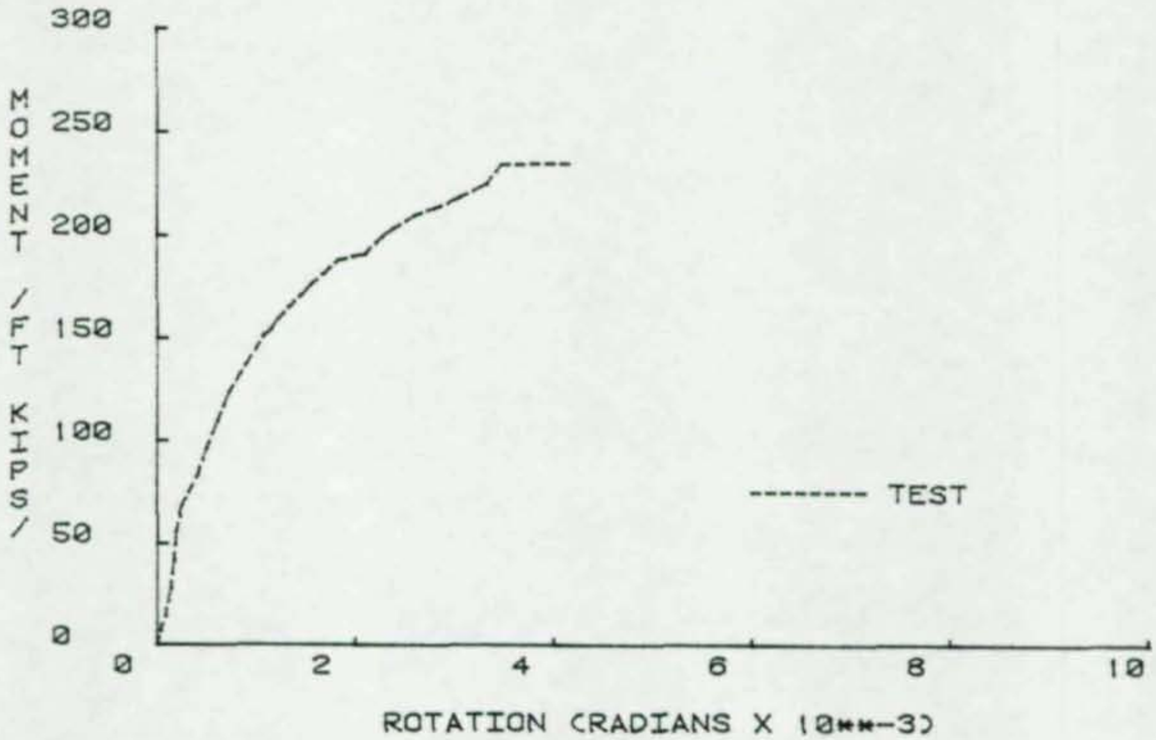

(e) End-Plate Moment versus Rotation

Figure D.1 Results from Test ES-3/4-7/16-20. Continued

APPENDIX E

ES-3/4-1/2-20 TEST RESULTS

TEST SYNOPSIS

PROJECT:	MBMA END-PLATE			
TEST:	ES-3/4-1/2-20			
TEST DATE:	7-31-85			
CONNECTION DESCRIPTION:	Four-bolt extended stiffened moment end-plate with a single row of two bolts each side of beam tension flange			
BEAM DATA:				
Depth	h	(in)	=	19.969
Flange width	bf	(in)	=	6.0
Web thickness	tw	(in)	=	0.225
Flange thickness	tf	(in)	=	0.483
Moment of inertia	I	(in**4)	=	679.0
END-PLATE DATA:				
Thickness	tp	(in)	=	0.476
Extension outside beam flange	Pext	(in)	=	2.937
Pitch to bolt from flange	Pf	(in)	=	1.580
Gage	g	(in)	=	3.500
Steel yield stress (measured)	Fpy	(ksi)	=	51.8
BOLT DATA:				
Type			=	A325
Diameter	db	(in)	=	0.750
Pretension force	Tb	(k)	=	28.0
PREDICTION:				
End-plate failure moment	Mu	(k-ft)	=	163.3
Bolt failure (proof) moment	Myb	(k-ft)	=	168.4
Beam failure moment		(k-ft)	=	294.1
EXPERIMENTAL:				
Maximum applied moment		(k-ft)	=	203.0
Moment at bolt proof load		(k-ft)	=	149.9
Maximum vertical centerline deflection		(in)	=	3.111
Maximum inner end-plate separation		(in)	=	0.14795
Maximum outer end-plate separation		(in)	=	0.11632

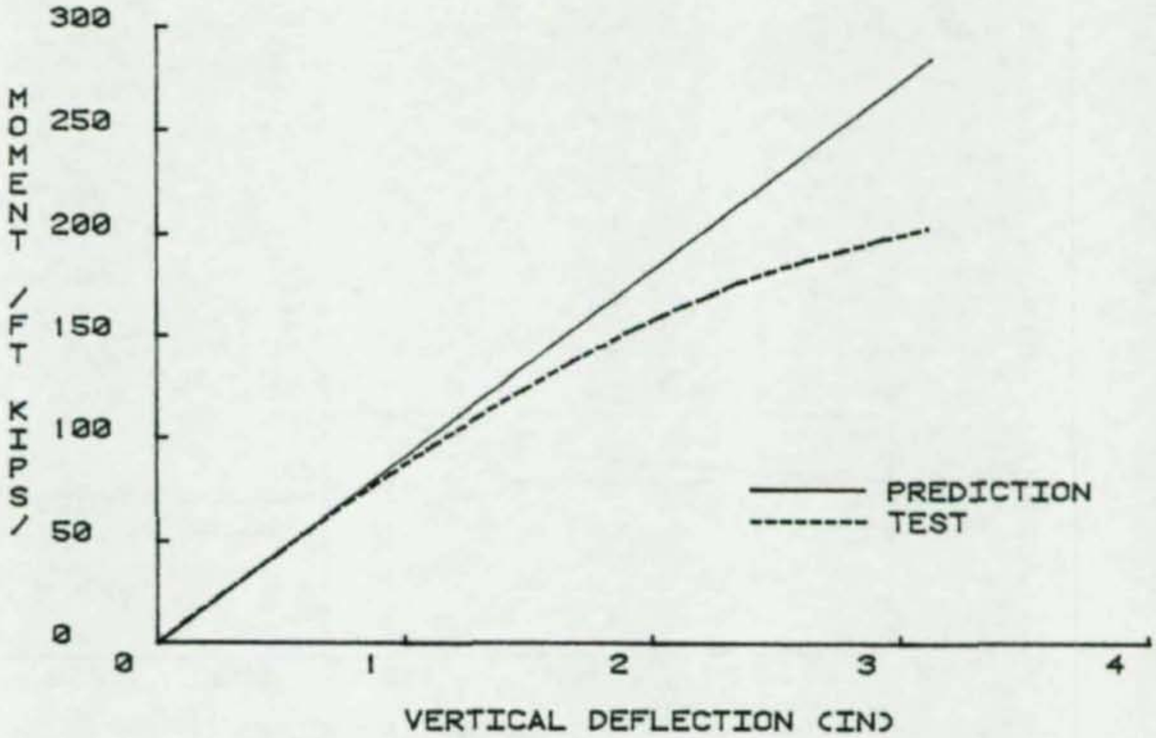

(a) End-Plate Moment versus Midspan Deflection

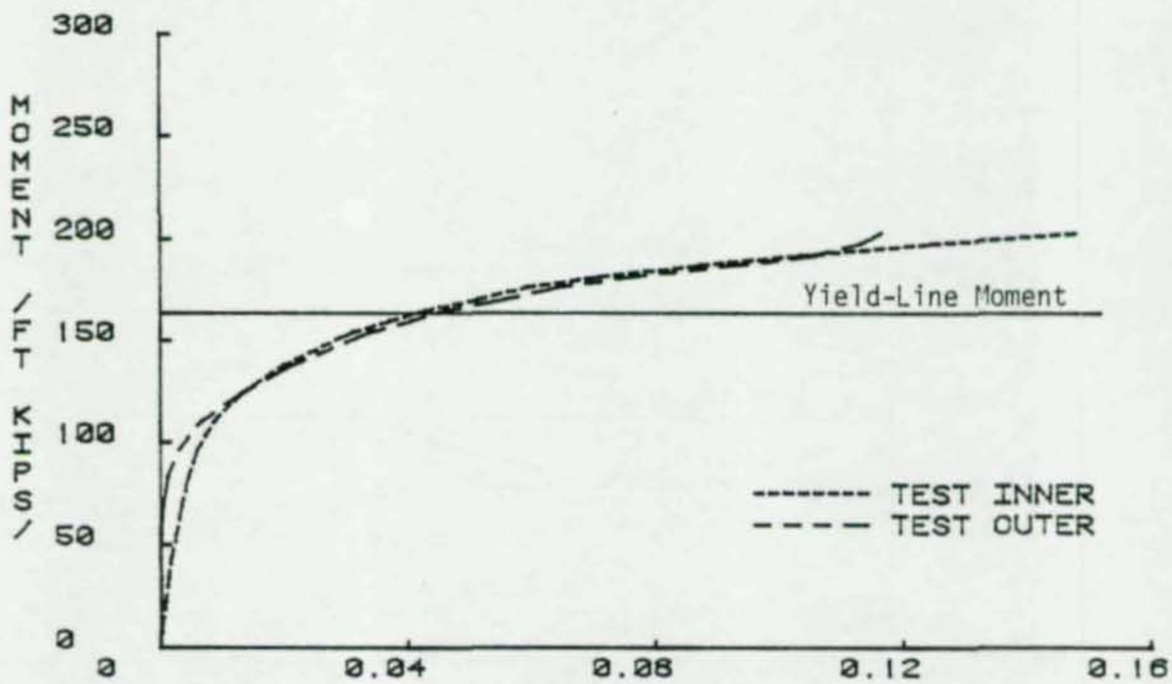

(b) End-Plate Moment versus Plate Separation

Figure E.1 Results from Test ES-3/4-1/2-20

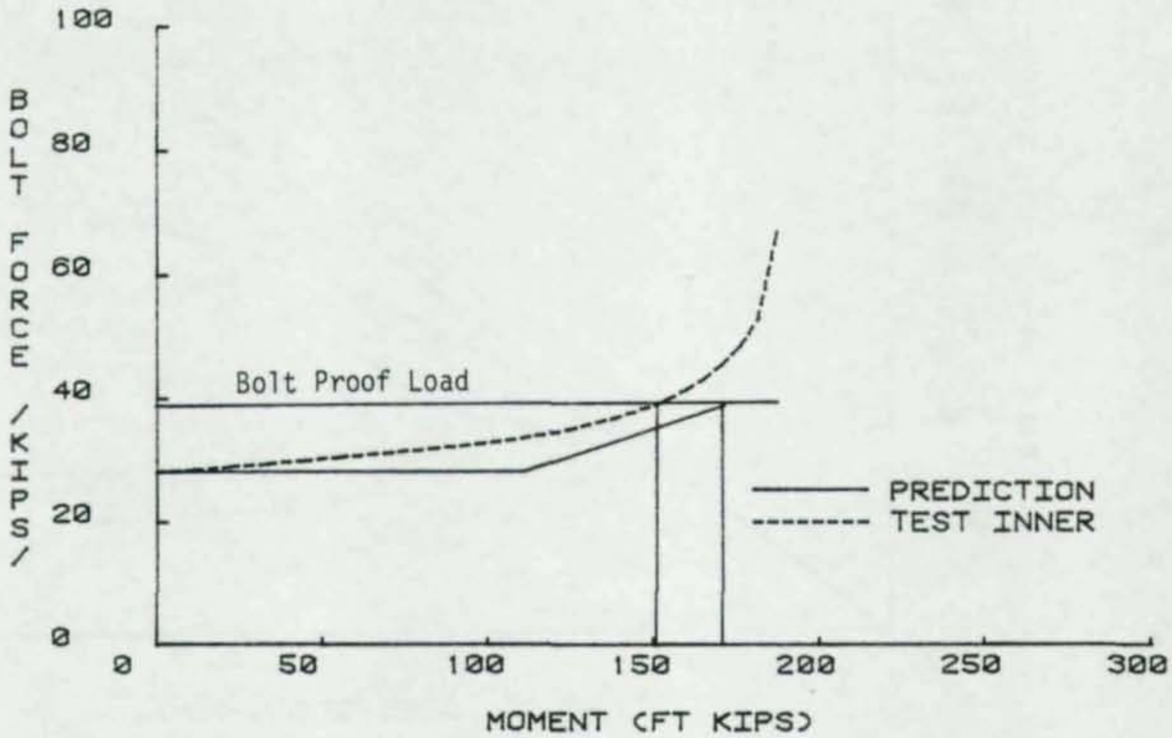

(c) Inner Bolt Force versus End-Plate Moment

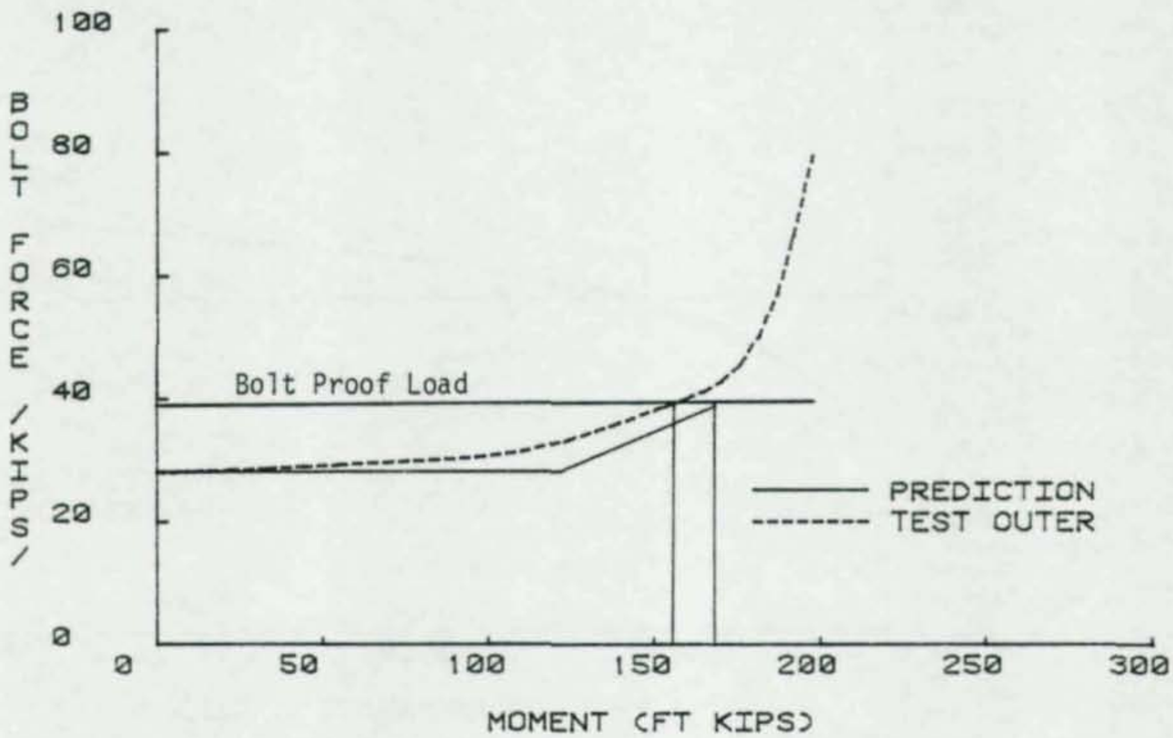

(d) Outer Bolt Force versus End-Plate Moment

Figure E.1 Results from Test ES-3/4-1/2-20. Continued

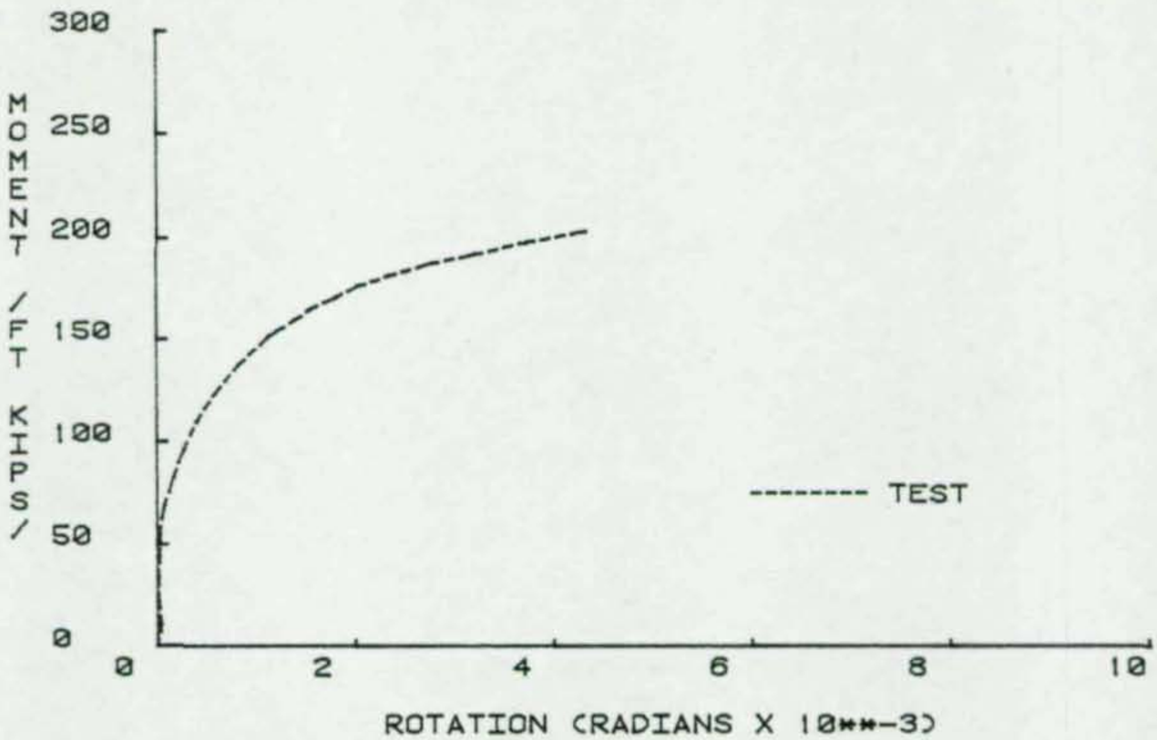

(e) End-Plate Moment versus Rotation

Figure E.1 Results from Test ES-3/4-1/2-20, Continued

APPENDIX F

ES-1-1/2-24 TEST RESULTS

TEST SYNOPSIS

PROJECT:	MBMA END-PLATE
TEST:	ES-1-1/2-24
TEST DATE:	8-20-85
CONNECTION DESCRIPTION:	Four-bolt extended stiffened moment end-plate with a single row of two bolts each side of beam tension flange

BEAM DATA:				
Depth	h	(in)	=	24.063
Flange width	bf	(in)	=	8.031
Web thickness	tw	(in)	=	0.234
Flange thickness	tf	(in)	=	0.496
Moment of inertia	I	(in**4)	=	1345.8
END-PLATE DATA:				
Thickness	tp	(in)	=	0.486
Extension outside beam flange	Pext	(in)	=	3.218
Pitch to bolt from flange	Pf	(in)	=	1.692
Gage	g	(in)	=	3.218
Steel yield stress (measured)	Fpy	(ksi)	=	51.6
BOLT DATA:				
Type			=	A325
Diameter	db	(in)	=	1.000
Pretension force	Tb	(k)	=	51.0
PREDICTION:				
End-plate failure moment	Mu	(k-ft)	=	249.8
Bolt failure (proof) moment	Myb	(k-ft)	=	283.2
Beam failure moment		(k-ft)	=	481.9
EXPERIMENTAL:				
Maximum applied moment		(k-ft)	=	349.5
Moment at bolt proof load		(k-ft)	=	330.8
Maximum vertical centerline deflection		(in)	=	3.849
Maximum inner end-plate separation		(in)	=	0.06804
Maximum outer end-plate separation		(in)	=	0.00336

DISCUSSION:

An instrumentation problem occurred with the caliper measuring outer end-plate separation. The maximum outer end-plate separation reported is smaller than that anticipated.

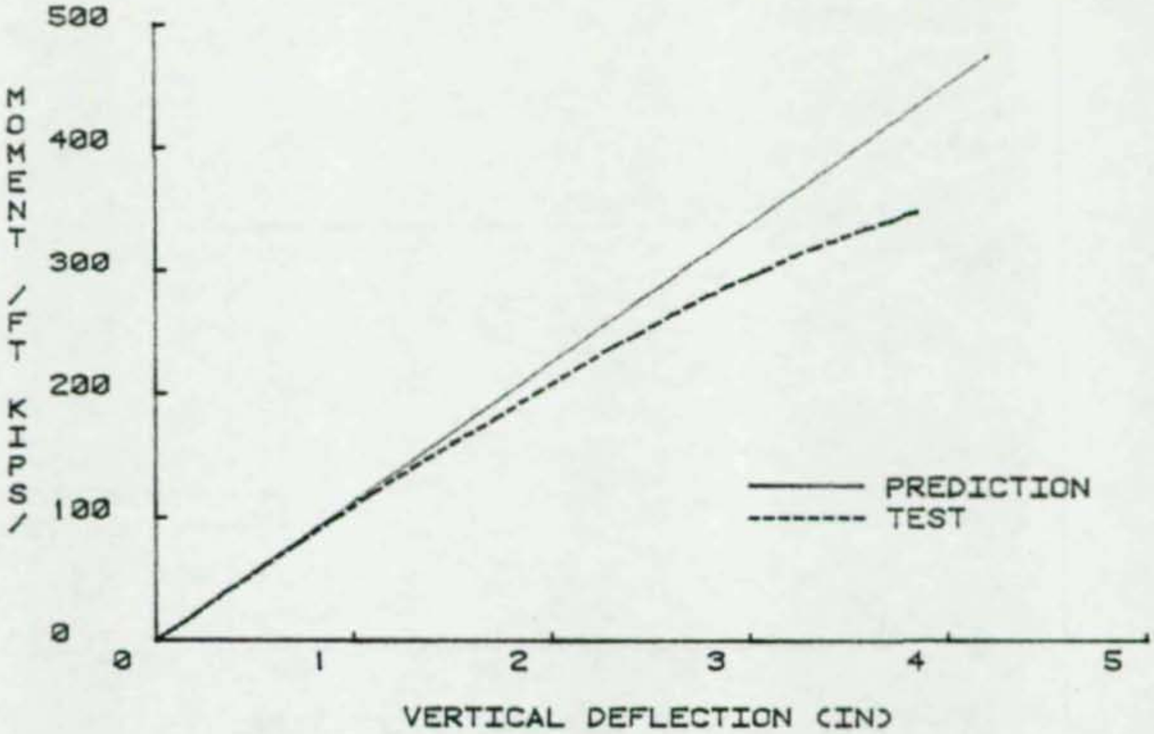

(a) End-Plate Moment versus Midspan Deflection

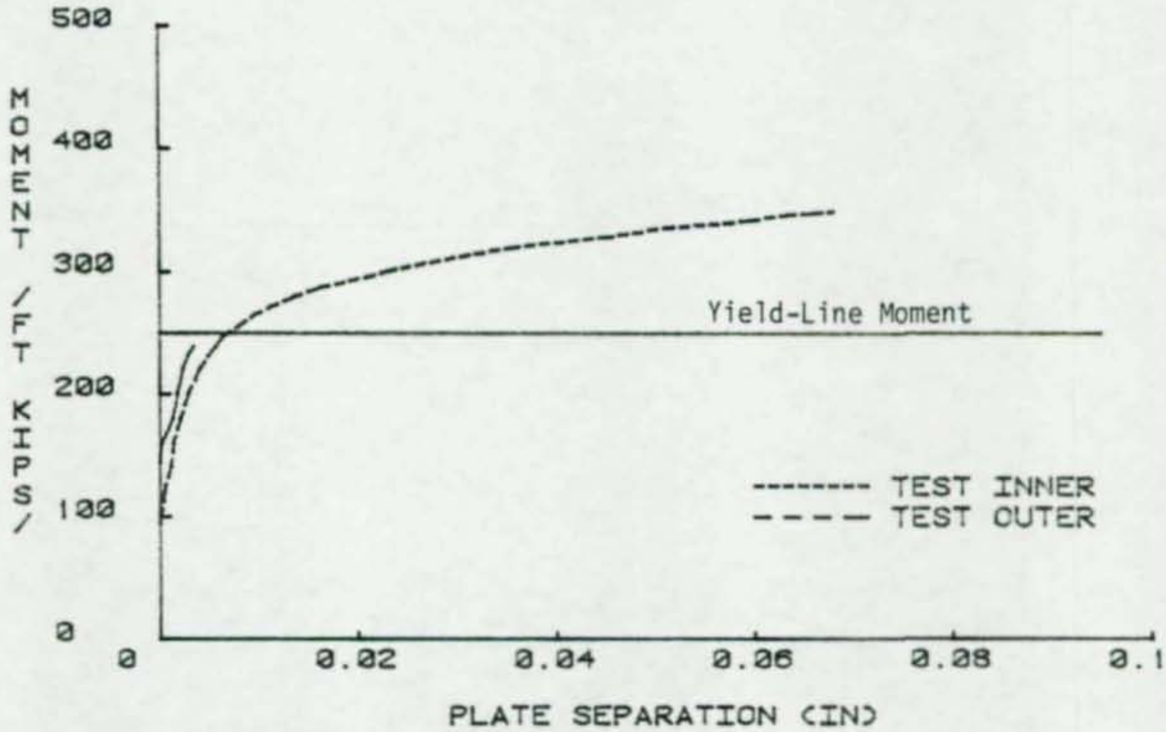

(b) End-Plate Moment versus Plate Separation

Figure F.1 Results from Test ES-1-1/2-24

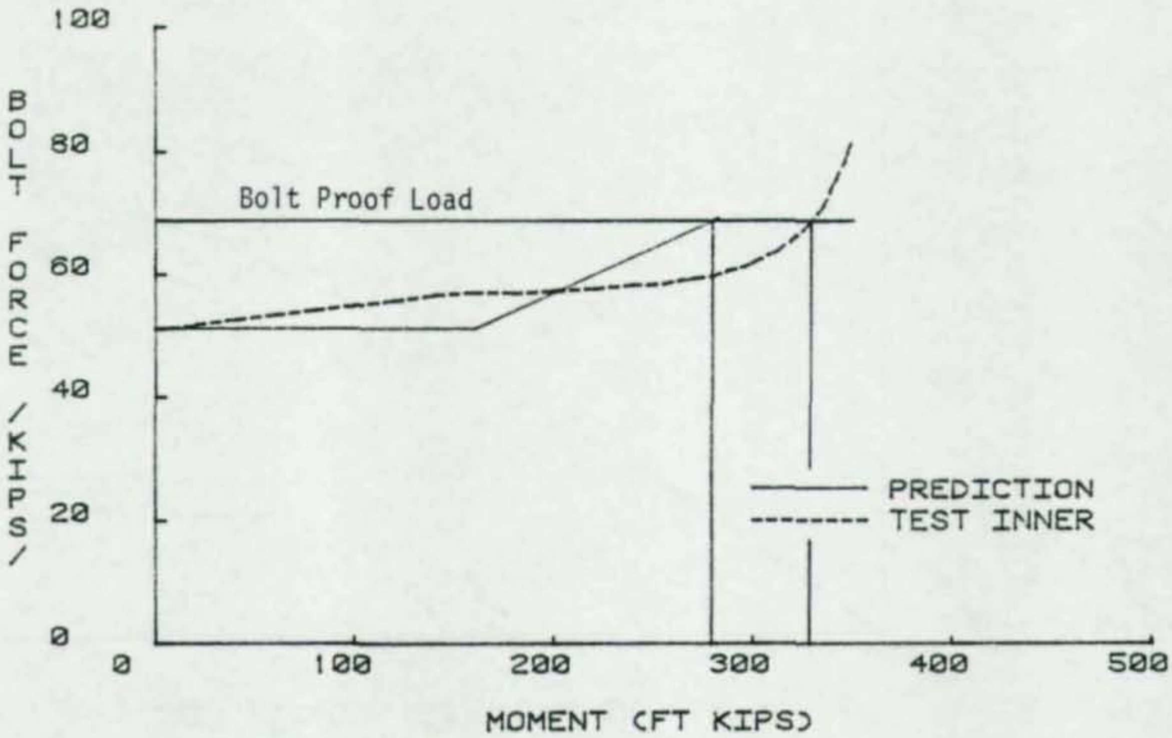

(c) Inner Bolt Force versus End-Plate Moment

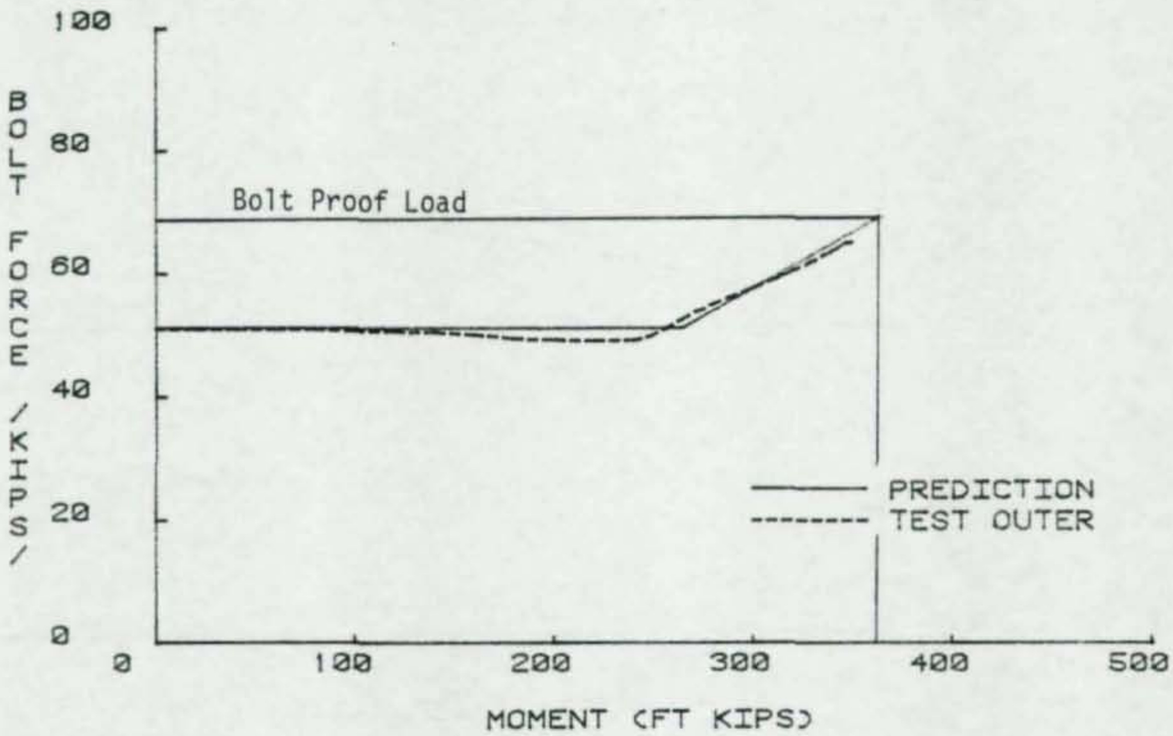

(d) Outer Bolt Force versus End-Plate Moment

Figure F.1 Results from Test ES-1-1/2-24, Continued

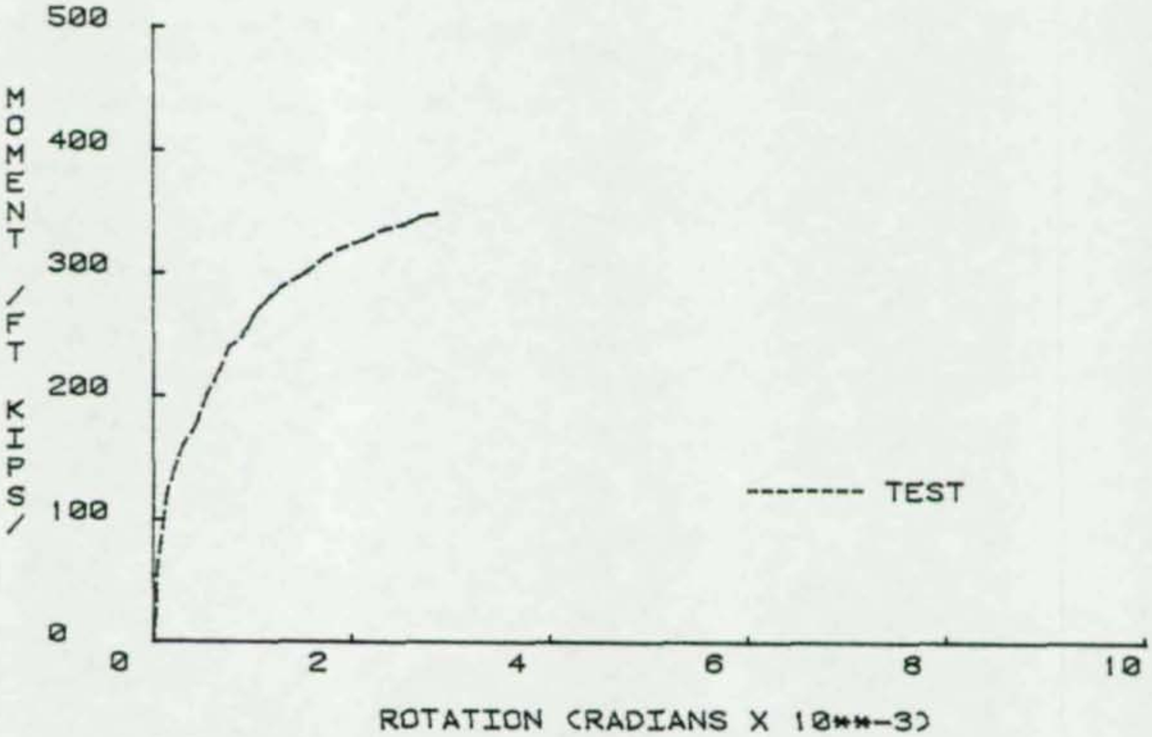

(e) End-Plate Moment versus Rotation

Figure F.1 Results from Test ES-1-1/2-24, Continued

APPENDIX G

ES-1-5/8-24 TEST RESULTS

TEST SYNOPSIS

PROJECT:	MBMA END-PLATE			
TEST:	ES-1-5/8-24			
TEST DATE:	8-26-85			
CONNECTION DESCRIPTION:	Four-bolt extended stiffened moment end-plate with a single row of two bolts each side of beam tension flange			
BEAM DATA:				
Depth	h	(in)	=	23.938
Flange width	bf	(in)	=	8.0
Web thickness	tw	(in)	=	0.496
Flange thickness	tf	(in)	=	0.496
Moment of inertia	I	(in**4)	=	1342.1
END-PLATE DATA:				
Thickness	tp	(in)	=	0.620
Extension outside beam flange	Pext	(in)	=	3.531
Pitch to bolt from flange	Pf	(in)	=	1.723
Gage	g	(in)	=	4.500
Steel yield stress (measured)	Fpy	(ksi)	=	52.7
BOLT DATA:				
Type			=	A325
Diameter	db	(in)	=	1.000
Pretension force	Tb	(k)	=	51.0
PREDICTION:				
End-plate failure moment	Mu	(k-ft)	=	364.5
Bolt failure (proof) moment	Myb	(k-ft)	=	333.6
Beam failure moment		(k-ft)	=	493.4
EXPERIMENTAL:				
Maximum applied moment		(k-ft)	=	379.4
Moment at bolt proof load		(k-ft)	=	301.6
Maximum vertical centerline deflection		(in)	=	4.014
Maximum inner end-plate separation		(in)	=	0.08714
Maximum outer end-plate separation		(in)	=	0.06421

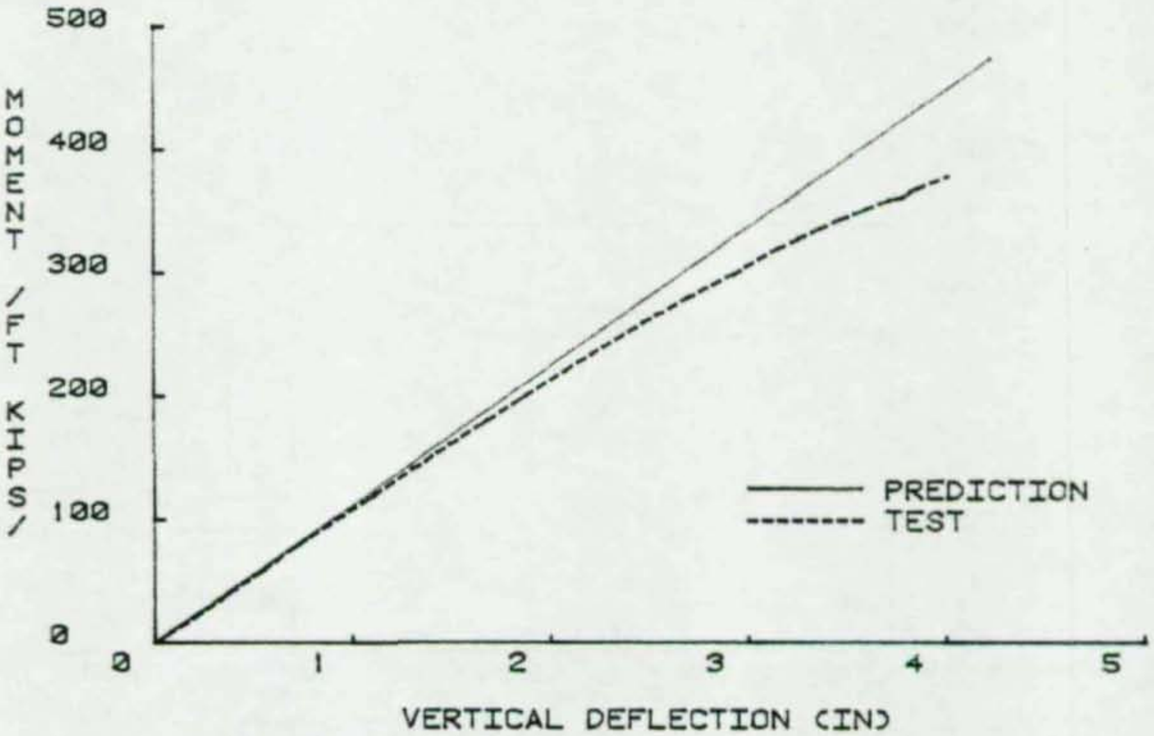

(a) End-Plate Moment versus Midspan Deflection

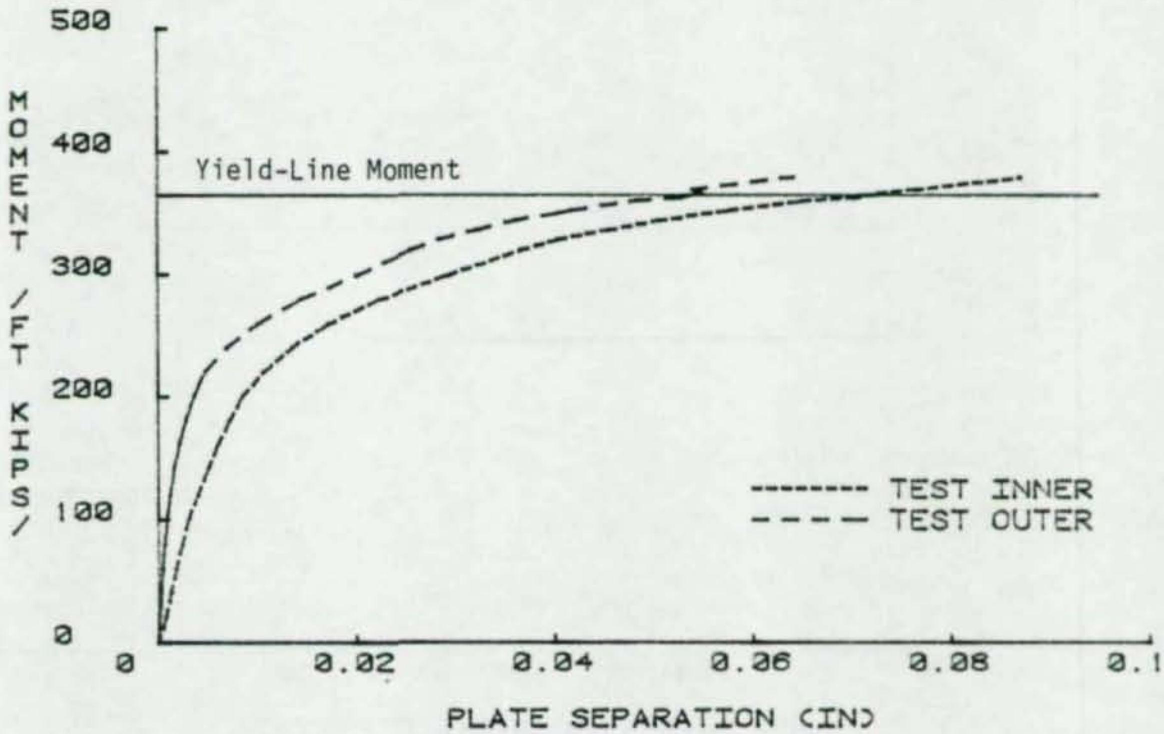

(b) End-Plate Moment versus Plate Separation

Figure G.1 Results from Test ES-1-5/8-24

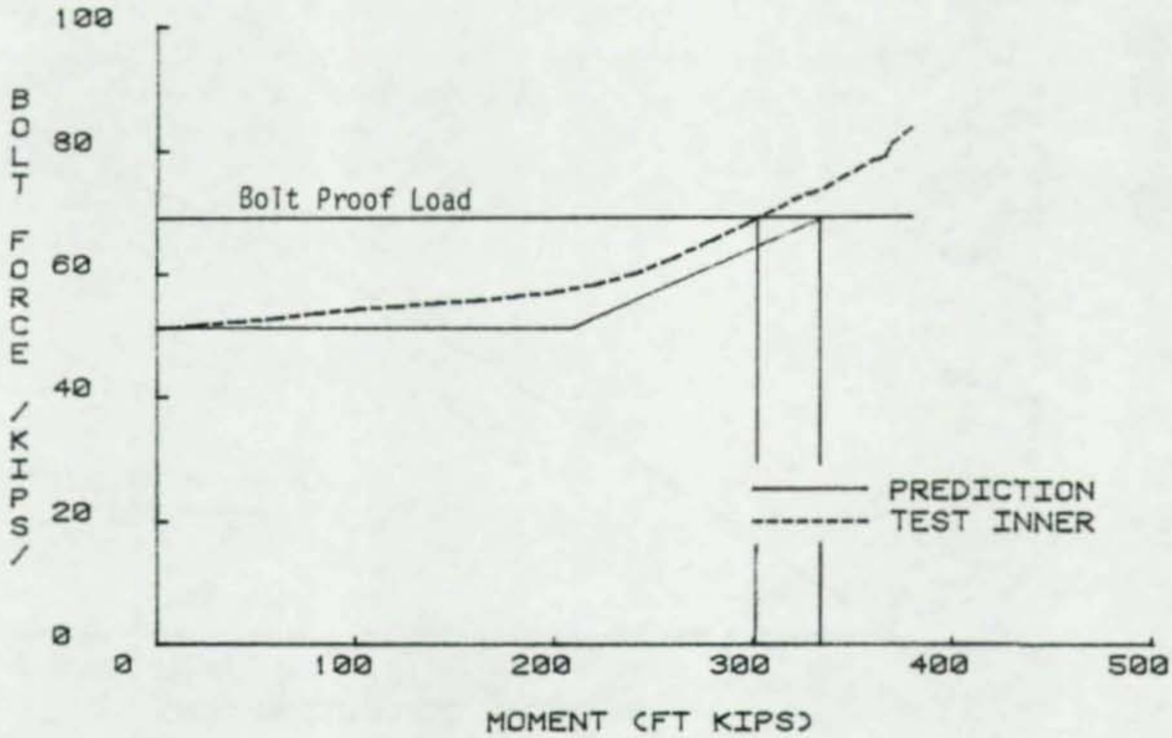

(c) Inner Bolt Force versus End-Plate Moment

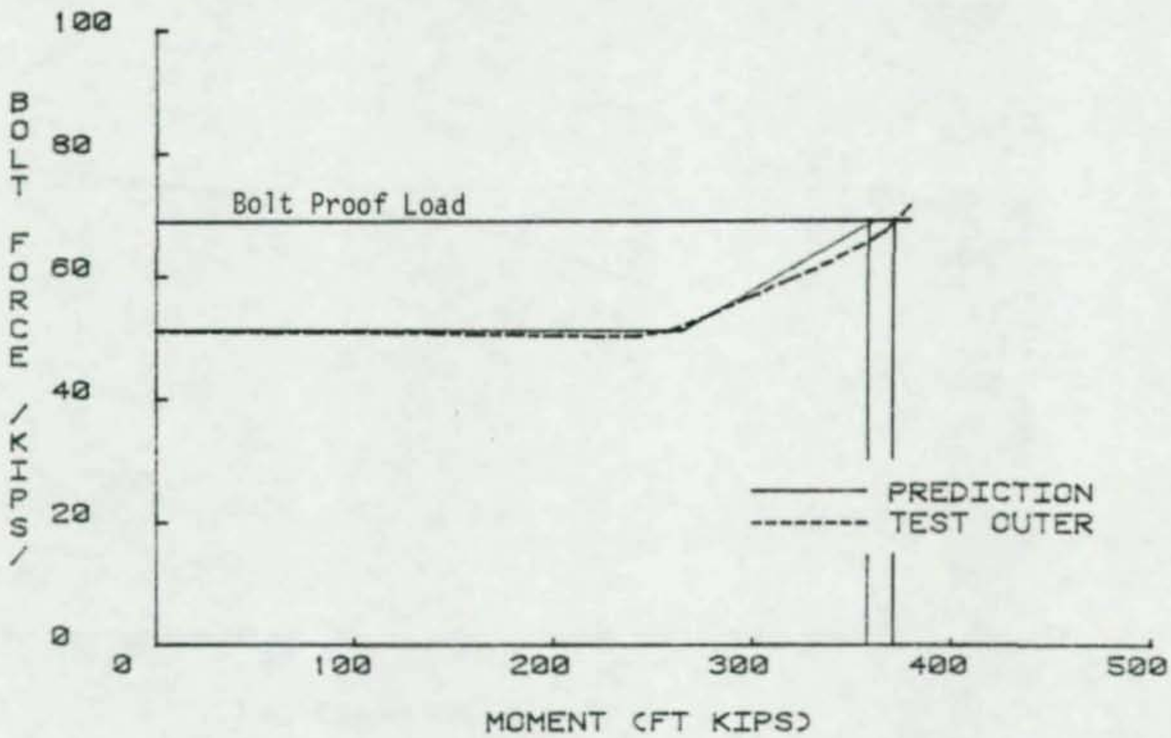

(d) Outer Bolt Force versus End-Plate Moment

Figure G.1 Results from Test ES-1-5/8-24, Continued

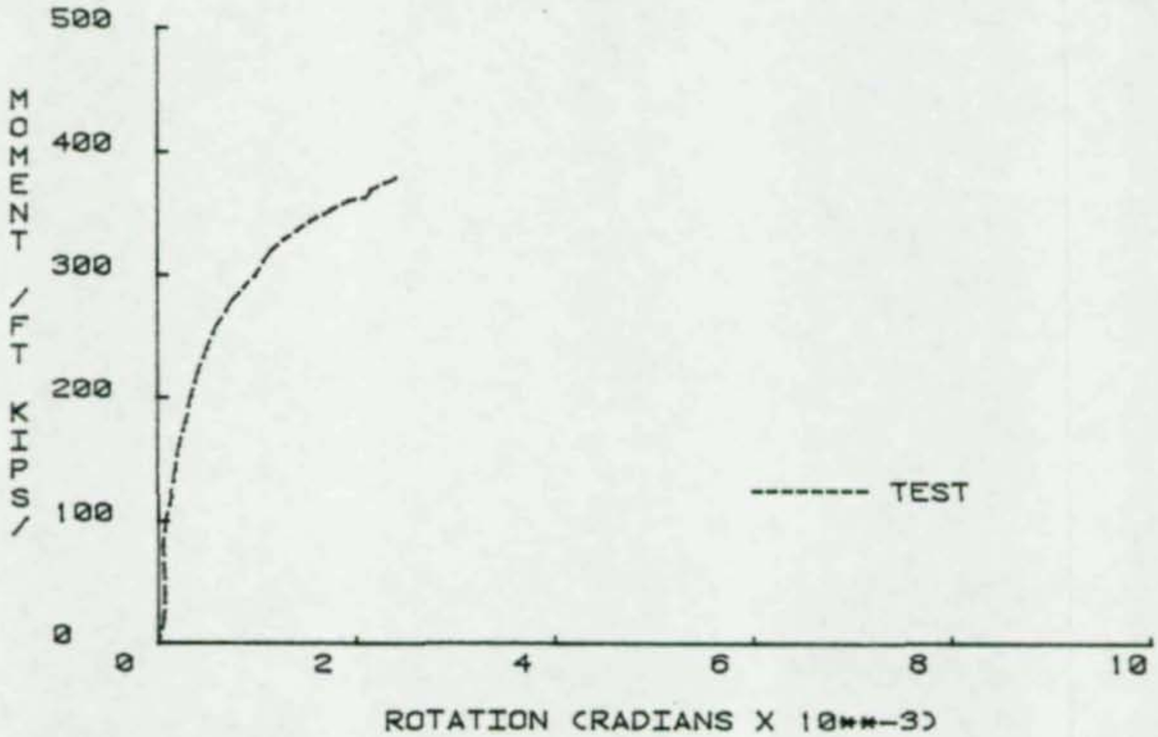

(e) End-Plate Moment versus Rotation

Figure G.1 Results from Test ES-1-5/8-24, Continued